(12)

PULSED LASER DEVICE DEVELOPMENT PROGRAM

VOLUME III OF IV

ABEL II SMALL-SCALE FLOW TEST REPORT

B. T. Vu

AVCO EVERETT RESEARCH LABORATORY, INC.
a Subsidiary of the Avco Corporation
2385 Revere Beach Parkway
Everett, Massachusetts 02149

June 1981

Final Technical Report
31 December 1979 – 30 September 1981

prepared for

HEADQUARTERS
U.S. ARMY MISSILE COMMAND
Redstone Arsenal, Alabama 35809

UNCLASSIFIED

SECURITY CLASSIFICATION OF THIS PAGE (When Data Enter

REPORT DOCUMENTATION P		READ INSTRUCTIONS BEFORE COMPLETING FORM
1 REPORT NUMBER	2 GOVT ACCESSION NO. AD-A127 925	3 RECIPIENT'S CATALOG NUMBER
4 TITLE (and Subtitle) Pulsed Laser Device Development Program Volume III of IV ABEL II Small-Scale Flow Test Report		5 TYPE OF REPORT & PERIOD COVERED Final Technical Report 12/31/79 - 9/30/81
		6 PERFORMING ORG. REPORT NUMBER
7 AUTHOR(s) B.T. Vu		8 CONTRACT OR GRANT NUMBER(s) DAAH01-80-C-0208
9 PERFORMING ORGANIZATION NAME AND ADDRESS Avco Everett Research Laboratory 2385 Revere Beach Parkway Everett, Mass. 02149		10 PROGRAM ELEMENT, PROJECT, TASK AREA & WORK UNIT NUMBERS CDRL Item A008
11 CONTROLLING OFFICE NAME AND ADDRESS Headquarters U.S. Army Missile Command Redstone Arsenal, Alabama 35809		12 REPORT DATE June 1981
		13 NUMBER OF PAGES 63
14 MONITORING AGENCY NAME & ADDRESS (if different from Controlling Office)		15 SECURITY CLASS. (of this report) Unclassified
		15a DECLASSIFICATION/DOWNGRADING SCHEDULE

16 DISTRIBUTION STATEMENT (of this Report)

Approved for Public Release; Distribution Unlimited

17 DISTRIBUTION STATEMENT (of the abstract entered in Block 20, if different from Report)

18 SUPPLEMENTARY NOTES

19 KEY WORDS (Continue on reverse side if necessary and identify by block number)

Electric Discharge Laser	Phase Aberration
Repetitively Pulsed	Beam Degradation
Gas Flow Interface	Velocity Shear
Turbulent Mixing Layer	Refractive Index

20 ABSTRACT (Continue on reverse side if necessary and identify by block number)

A series of experiments were performed to study laser beam degradation for propagation normal to two-dimensional turbulent mixing layers.

An analytical expression for beam degradation, derived earlier, is verified by the experiments. The expression shows that beam degradation is proportional to the square of the mixing layer thickness, L, and the square of the refractive index –

DD FORM 1 JAN 73 1473 EDITION OF 1 NOV 65 IS OBSOLETE

UNCLASSIFIED

SECURITY CLASSIFICATION OF THIS PAGE (When Data Entered)

20. difference, Δn, between the two fluids across the layer. For a fixed Δn, degradation is thus dependent on L.

In these experiments, the effects of free-stream characteristics and velocity shear on the mixing layer growth rate were studied. For layers with gas streams issuing from an orifice plate, the growth rate is high due to large turbulence and large non-uniformities in the free streams. A fine mesh screen positioned over the flow plate is quite effective in reducing the mixing layer growth. Mixing layer bending, which is most severe in the jetting region near the orifice plate, is also minimized by screening.

The effect of shear on the mixing layer growth rate was studied for moderate shear. It was found that the growth rate is a function of the shear ratio R proposed by Sabin and Abramovich. For $R < 0.1$, a low growth rate of 5% can be achieved by screening.

SUMMARY OF REPORT VOLUMES

This document is one of four volumes which, collectively, comprise the Final Technical Report for the Pulsed Laser Device Development Program, also known as ABEL II (ABEL is an acronym for Air-Breathing Electric Laser). Volume I delineates the contract technology development effort on a by-task basis and references the three major experimental activities described separately in Volumes II, III and IV.

Volume I - ABEL II Technology (Confidential)

Volume II - ABEL II Average Power/Low Power Test Report (Confidential)

Volume III - ABEL II Small-Scale Flow Test Report (Unclassified)

Volume IV - ABEL II Preliminary Beam Quality Test Report (Unclassified)

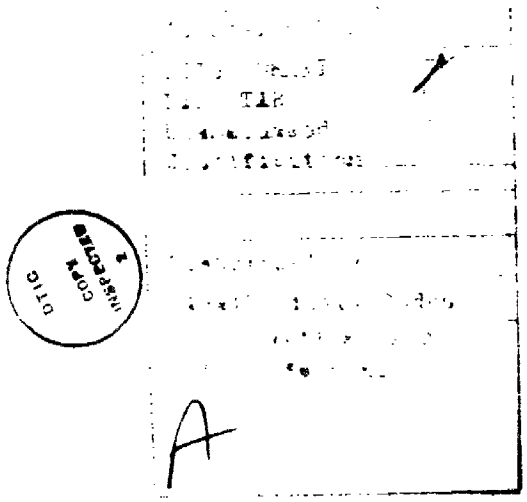

TABLE OF CONTENTS

LIST OF ILLUSTRATIONS

1.0 INTRODUCTION

In the ABEL device, the laser beam must pass through an interface between two flowing gases of different indices of refraction, the main laser gas and nitrogen in the end flow, as illustrated in Figure 1. Inhomogeneous turbulent mixing in the interface causes phase aberration and degradation of the laser beam.

If the amount of phase aberration $\overline{\psi'^2}$ is small, the beam degradation is given by:[1]

$$\frac{\Delta I}{I_o} = \frac{I - I_o}{I_o} = \overline{\psi'^2} \tag{1}$$

where I and I_o are the degraded and nondegraded beam intensities respectively. A theoretical expression of the beam degradation due to turbulence has been derived:[2]

$$\frac{\Delta I}{I_o} = \overline{\psi'^2} = 2\left(\frac{2\pi}{\lambda}\right)^2 \Delta n^2 \alpha^2 L\ell \tag{2}$$

where λ is the laser wavelength, Δn is the refractive index difference across the mixing layer; α is an average scalar fluctuation intensity, L is the mixing layer thickness and ℓ is the turbulent macroscale related to the refractive index fluctuation.

Experimental studies on beam degradation across a turbulent mixing layer were carried out in a small-scale flow test in which the mixing layer was observed in a 20 cm high optical chimney.

---

1. Born, M. and Wolf, E., Principles of Optics, Permagon Press, 1975, pp. 463-465.

2. Vu, B.T., Sutton, G., Theophanis, G. and Limpaecher, R., "Laser Beam Degradation Through Optically Turbulent Mixing Layers," AIAA Paper 80-1414, 13th AIAA Fluid and Plasma Dynamics Conference, Snowmass, Colorado, 1980

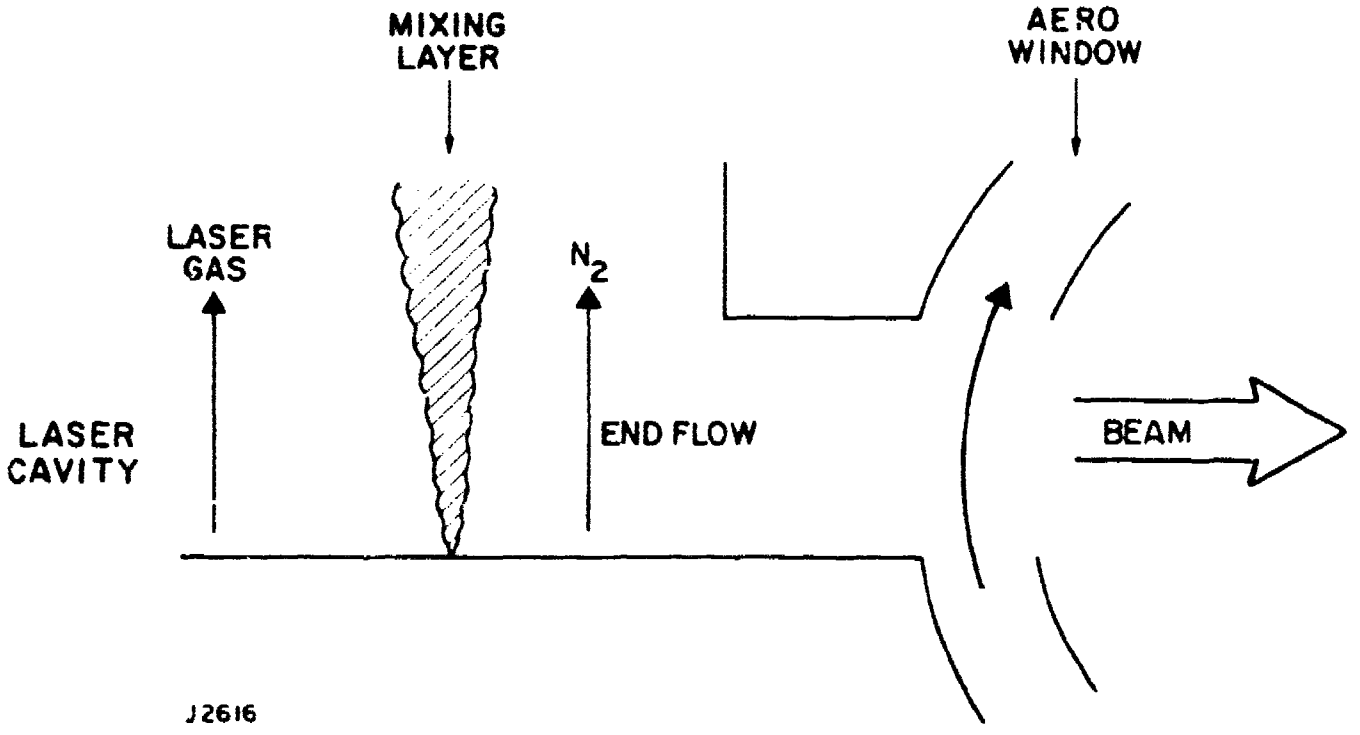

Figure 1 End Flow Mixing Layer

The four specific objectives of the test were:

1) to obtain experimental verification of the theoretical expression for beam degradation due to turbulence (Eq. 2),

2) to study beam degradation characteristics and mixing layer growth under velocity sheared conditions,

3) to test a method for reducing the beam degradation of a single layer by reducing the mixing layer growth, and

4) to study the mixing layer stability if one stream is exposed to a region of stagnant fluid, as in the case of the end flow shown in Figure 1.

Four series of experiments were carried out in connection with the four above objectives.

2.0 TEST APPARATUS

2.1 EXPERIMENTAL APPARATUS

Experiments at room temperature were carried out for a mixing layer between a stream of nitrogen and a stream of a mixture of helium and nitrogen. Mach-Zehnder interferometer data together with temperature and velocity data were obtained.

The flow setup is shown in Figure 2 and is described in detail elsewhere.[3] The two streams of gases divided by a splitter plate in a plenum chamber, passed through a flow plate and were allowed to mix in an optical chimney 7.11 cm long, 5.08 cm wide and 20.0 cm high. Two types of flow plates were used in the experiments and are shown in Figures 3a and 3b. The flow plate shown in Figure 3a is identical to that of the ABEL laser; the modified form shown in Figure 3b, had a small-mesh screen positioned over the orifice plate whose dimensions are shown in Figure 3c. Proper construction of the modified flow plate is important and is described in more detail in Section 4.3. The plenum chamber pressures were measured by two pressure gauges with 60 psig maximum pressure and 0.2 psi subdivisions. The pressures were constant within 0.5 psi for each experimental run. The velocities of the gases in the optical chimney were measured with a hot-wire anemometer and were also cross checked against predictions from the plenum pressures as discussed in Section 2.2. Temperatures of both streams were measured in the chimney. They were constant for all gases used and were about 3°F below room temperature.

2.2 CALIBRATION

Gas velocity measurements were made with a hot-wire anemometer (Thermal Science, Inc 1050) and a standard hot-film sensor (TSI/1210-20 Sensor, 0.002" dia., 0.06" long, frequency response 250 kHz). The hot-film sensors were calibrated with nitrogen flow, helium flow and five mixtures of nitrogen and helium. Typical calibration curves are shown in Figure 4.

---

3. "Cold Flow Electric Laser Development (U)", ABEL I Final Technical Report for Period 1 Jan. 1977 - 30 Sept. 1979, Army MICOM Contract DAAK40-75-C-1272, AERL Doc. 79-320, October 1979. CONFIDENTIAL

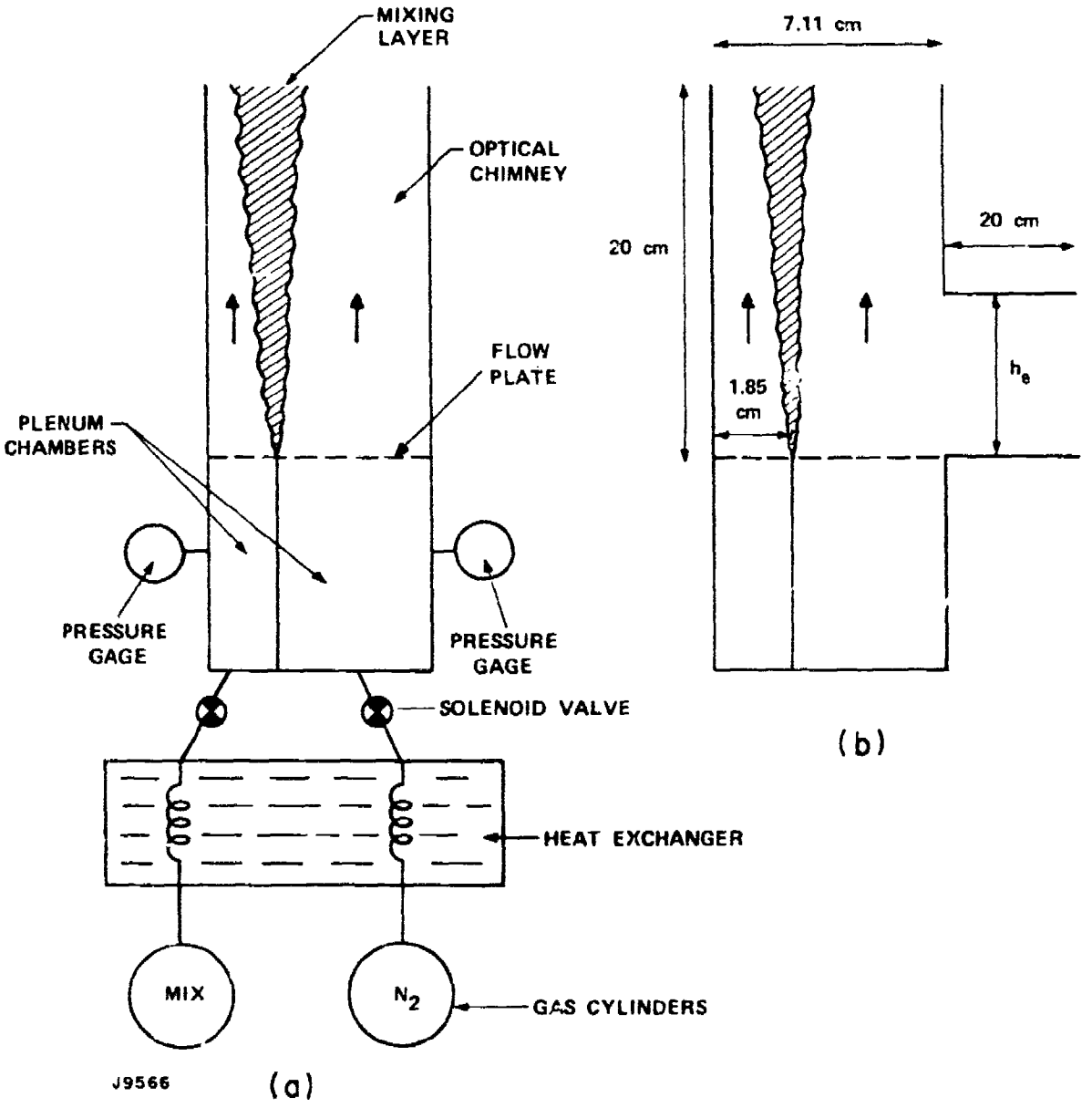

Figure 2 Flow System and Control (a) and Optical Chimney for Experimental Series #4 (b)

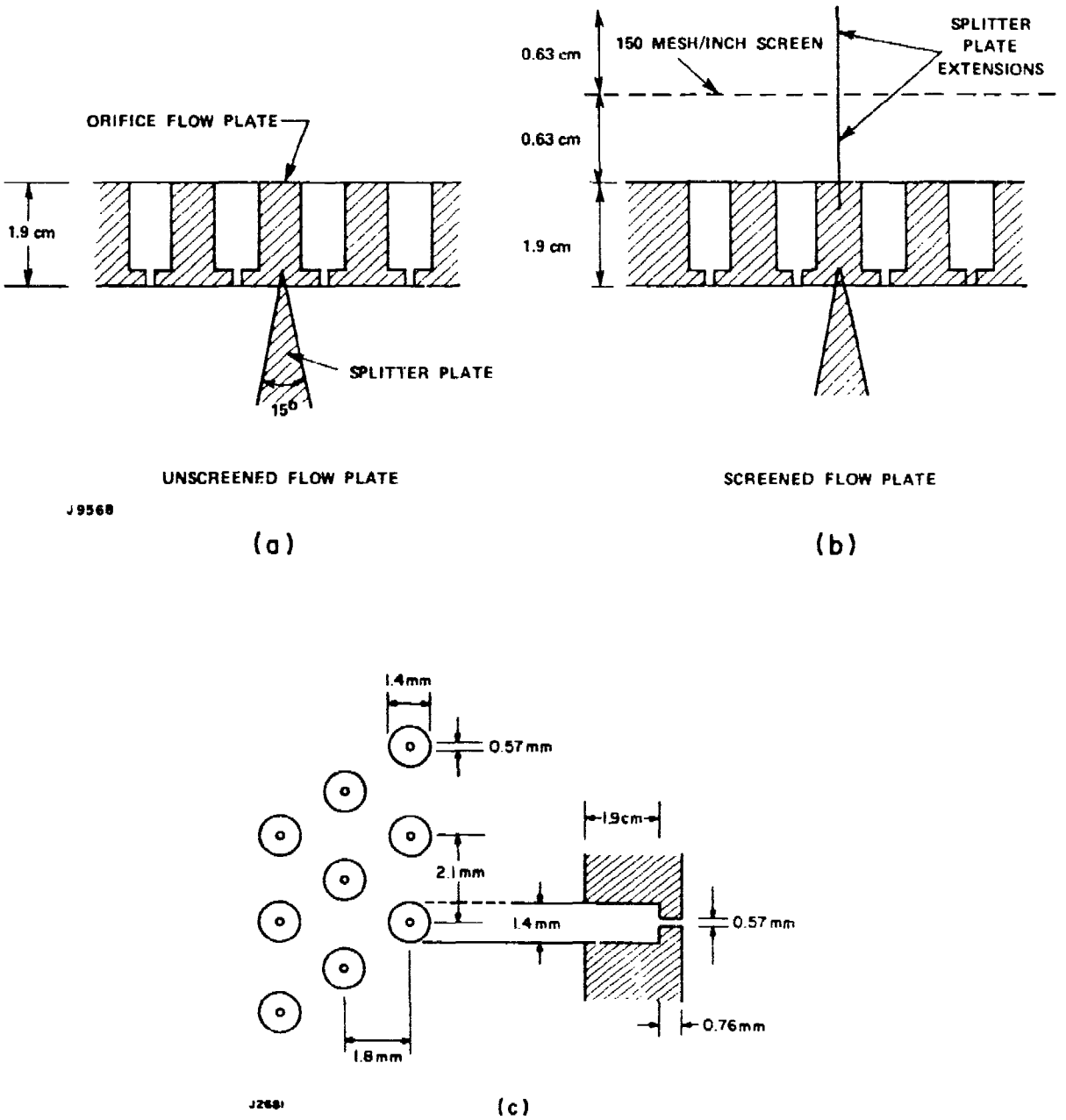

Figure 3 Flow Plate Configuration: (a) Unscreened, (b) Screened and (c) Dimensional Details

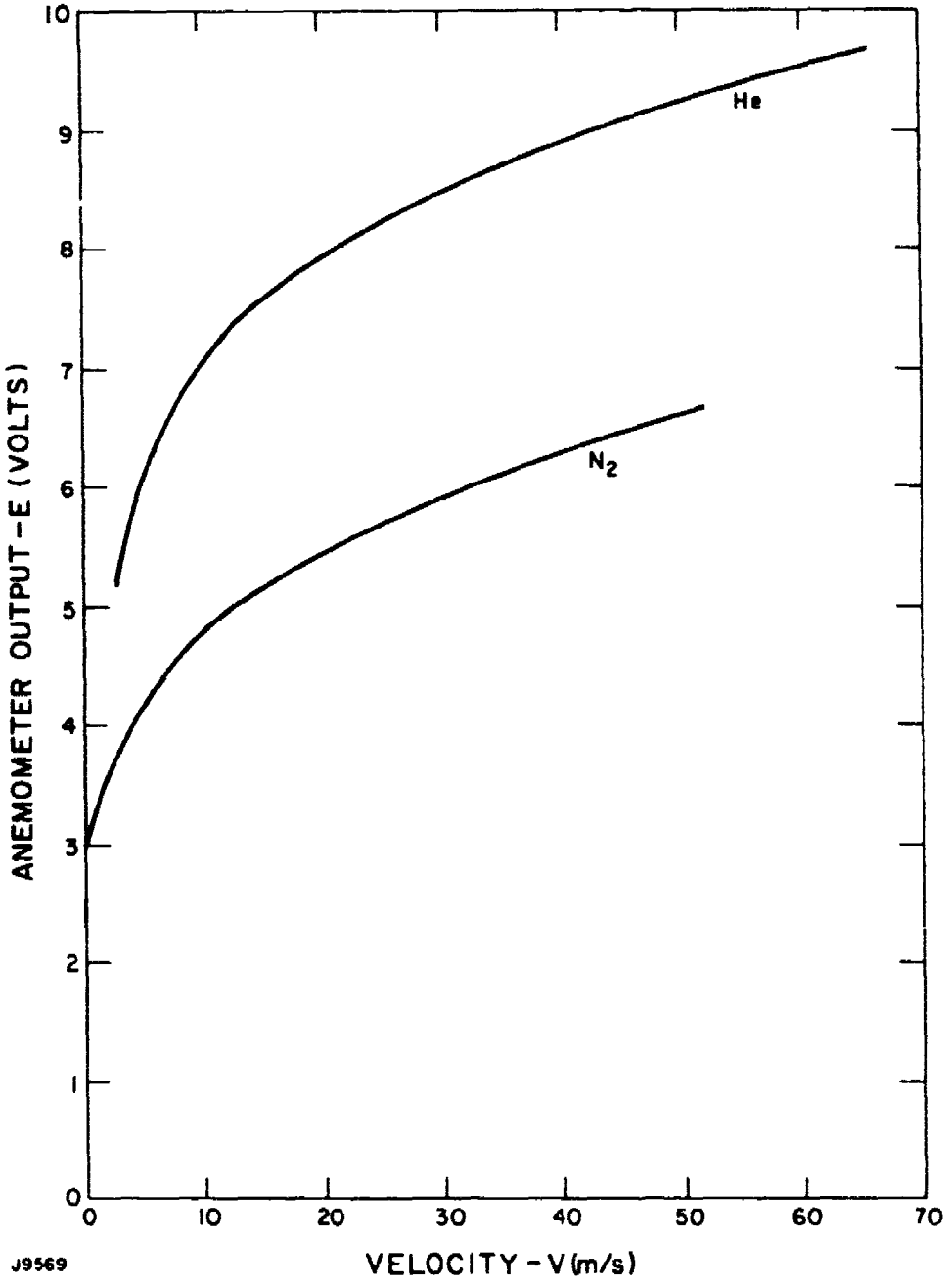

Figure 4 Hot-Film Calibration Curves

The velocity of each stream measured by the hot-film sensor averaged across the flow plate was correlated with the plenum pressure. Figure 5 shows the calibrated data for different gas mixtures at different plenum pressures. The solid lines in the figure represent theoretical velocities calculated from the plenum pressures. The theoretical calculations are based on subsonic and choked flow through the orifice plate.

For subsonic flow, the velocity in the chimney is

$$V = C_d \frac{A_o}{A} \sqrt{2 \frac{(P_o - P)}{P} \frac{RT}{M}} \qquad (3)$$

where

C_d is the discharge coefficient

A_o/A is the open-area ratio of the flow plate

P_o is the plenum pressure

P is the static pressure of the gas in the optical chimney

R is the universal gas constant (8314 J/kg mole)

M is the molecular mass (kg/kg mole)

T is the gas temperature (°K)

If the plenum pressure is larger than the critical pressure

$$P_o \geq \left(\frac{\gamma + 1}{2}\right)^{\frac{\gamma}{\gamma - 1}} (P) \qquad (4)$$

where γ is the ratio of the specific heats C_P/C_V, then the sonic choked flow relation applies

$$V = C_d \frac{A_o}{A} \left(\frac{\gamma R}{M T_o}\right)^{1/2} T \left(\frac{2}{\gamma + 1}\right)^{K/2} \frac{P_o}{P} \qquad (5)$$

where

T_o is the total temperature of the gas (°K)

T is the static temperature of the gas in the optical chimney

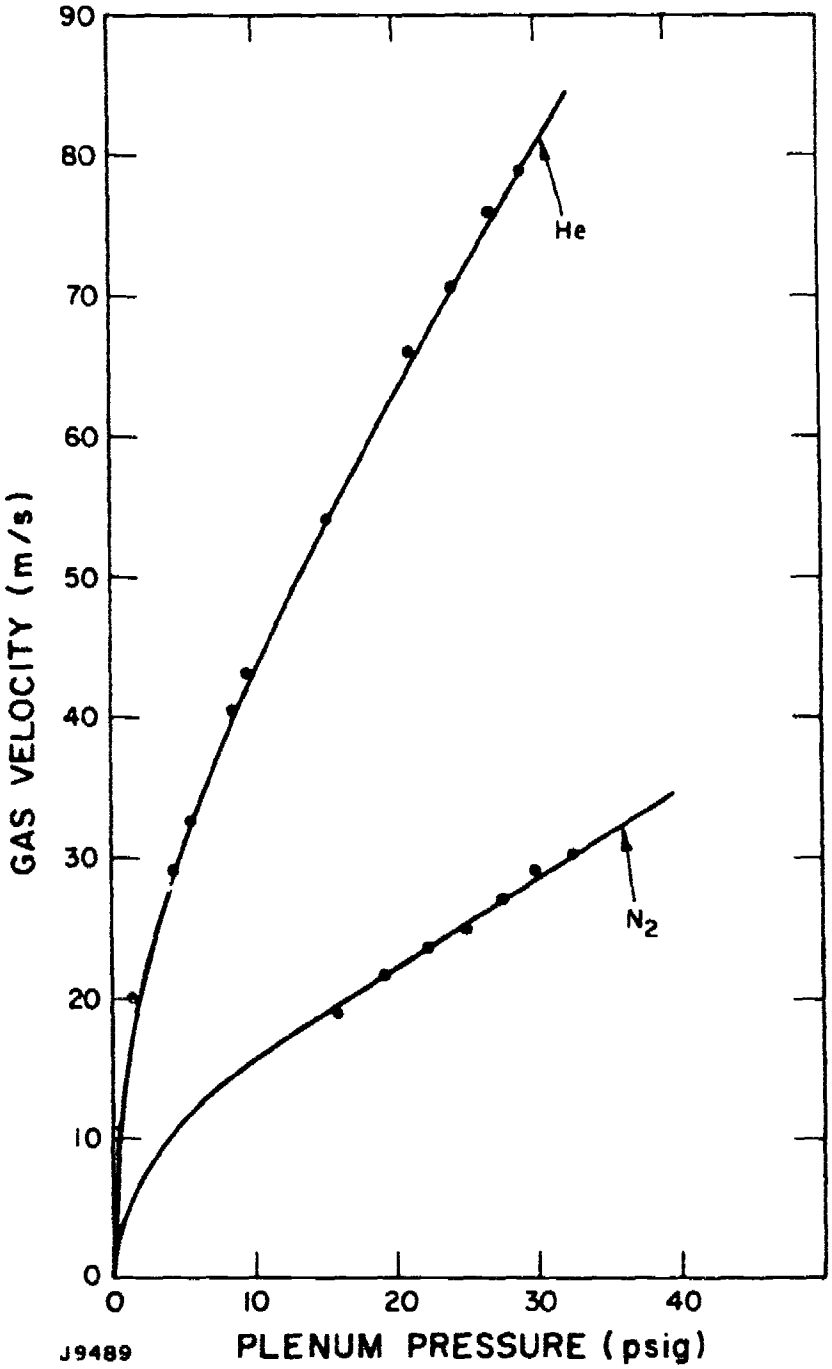

Figure 5 Flow Plate Calibration

K is $(\gamma + 1)/(\gamma - 1)$

To simplify calculations, we take A_o/A as the open-area ratio for the orifice plate alone which is 6.7%. Flow plate calibration is obtained with hot-wire anemometer measurements (Fig. 5), and the nominal discharge coeffients are found to be:

$$C_d = 0.69 \pm 3.5\%,$$

for the screened flow plate,

and $$C_d = 0.79 \pm 5\%,$$

for the unscreened flow plate.

3.0 TEST DESCRIPTION

3.1 PROCEDURE

The two principal test measurements were the beam degradation measurement and the mixing layer growth rate. These two measurements must be related to the gas velocities and the refractive index difference (or gas mixture composition) across the mixing layer.

The velocities were either measured by hot-wire anemometry or calculated using Eq. (3) and Eq. (5) with the measured discharge coefficients. For hot-wire measurements, the errors were about 2%, while velocities calculated from plenum pressures had uncertainies of about 5%.

The refractive index difference was measured directly from the interferograms, with the probe beam oriented parallel to the mixing layer. The fringe shift across the mixing layer was obtained by comparing a tare interferogram without flow and a disturbed interferogram with flow. The number of shifted fringes ΔJ is related to the difference in refractive index Δn as

$$\Delta J = \frac{\Delta n}{\lambda} W \tag{6}$$

where λ is the laser wave length (5260 Å) and W is the width of the optical chimney in the optical axis. With W = 5.08 cm for our experiment,

$$\Delta n = \Delta J \times 1.04 \times 10^{-4}$$

If the mixing layer is between a stream of nitrogen and a stream of a mixture of nitrogen and helium, both at temperature T (^{o}K) and 1 atm., then the mixture composition and the refractive index difference are related by:

$$\Delta n = (\beta_{N_2} - \beta_M) \frac{273}{T} \tag{7}$$

where β_{N_2} and β_M are the Gladstone-Dale constants for nitrogen and the mixture respectively. The constant β_M is given by

$$\beta_M = X_{N_2} \beta_{N_2} + X_{He} \beta_{He} \tag{8}$$

where X_i and β_i are respectively the molecular fraction and the Gladstone-Dale constant of species "i". Figure 6 shows Δn and the normalized velocity of the N_2/He mixture under sonic conditions as a function of composition.

3.2 DATA ANALYSIS

The interferogram data reduction was done by the following methods. First, the mixing layer growth was studied by orienting the probe beam parallel to the layer. If the profile of the average refractive index $\bar{n}$ in the mixing layer is given by the error function, we can define the mixing layer thickness L as the maximum slope thickness.[2] Figure 7 illustrates this method and shows that at the edge of this thickness, $\bar{n}$ differs from the value of $\bar{n}$ in the free stream by 0.105 Δn. From the disturbed interferogram, we can thus determine the edge of maximum slope thickness of the mixing layer. This method of determining the thickness is more accurate and objective than the "visual" determination of the mixing layer thickness base on shadowgraphs such as used by Brown and Roskho.[4] The visual method usually gives an overestimation for a mixing layer with larger Δn as compared to a mixing layer with small Δn.

Second, the value of beam degradation across the layer is determined from interferograms taken with the probe beam oriented perpendicular to the mixing layer. It is convenient to deal with the square root of the beam degradation or the RMS of the phase aberration, $\sqrt{\psi'^2}$, since they are linearly proportional to Δn and the thickness, L, of the mixing layer. The RMS phase aberration is obtained by the following method. A portion of the disturbed interferogram is first digitized. The linear dimensions of the analyzed area of the interferogram are chosen to be at least ten times the turbulent macroscale. With the fringes numbered consecutively, the digital data are the x-y coordinates of the intersection of the fringes with the reference lines drawn nearly perpendicular to the fringes, the distances between consecutive reference lines are chosen to be comparable to the fringe spacings. Computer analysis of the digital data were done with a computer code developed by the Optical Sciences Center (OSC) at the University of Arizona. A detailed description of the OSC code is given in the Appendix A. The program takes the (x,y) array points and fits them to a polynomial of the form

$$f(x,y) = Ax + By + C + D(x^2 + y^2) \qquad (3)$$

4. Brown, G.L. and Roshko, A., "On Density Effects and Large Structure in Turbulent Mixing Layers," J.F.M. Vol. 64, 1974, pp. 775-816.

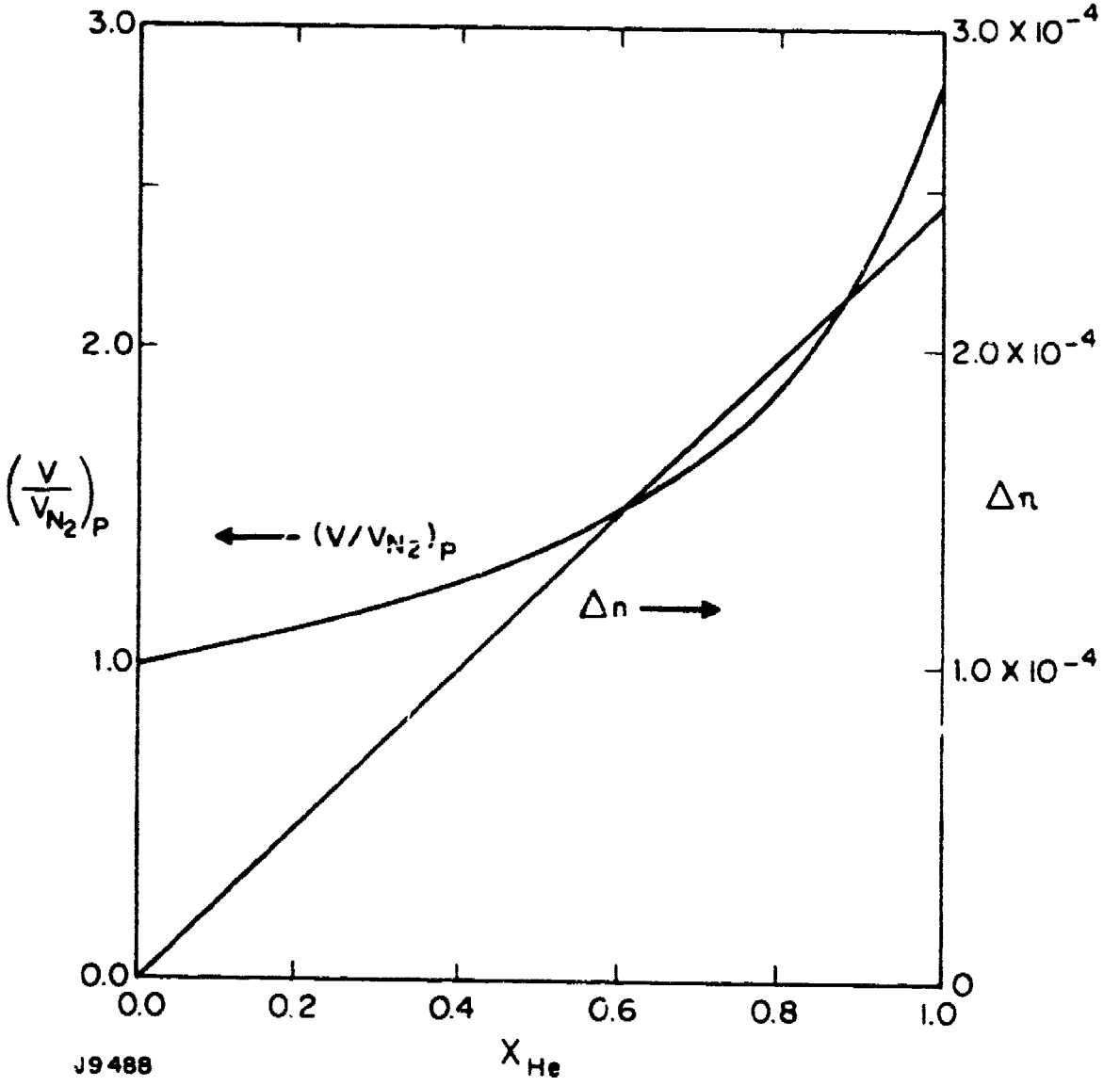

Figure 6 Velocity Ratio and Δn Versus Gas Composition; $(V/V_{N_2})_P$ is Ratio of Gas Mixture Velocity to Nitrogen Velocity Under Same Plenum Pressure

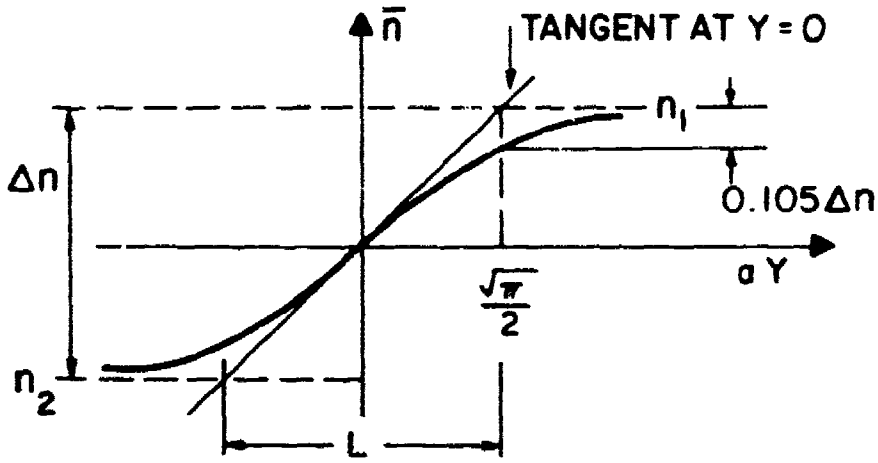

$$\frac{\bar{n}}{n_1} = \frac{1}{2}\left(1 - \frac{n_2}{n_1}\right)\left(\text{erf}\left[\alpha(x)y\right] - 1\right) + 1 \quad \text{(see ref. 2)}$$

Figure 7 Mixing Layer Thickness

using the least-square method. The first three terms represent the tilt; while the last term gives the defocus. The aberration given by f(x,y) from a plane is deterministic and does not contain any perturbation due to turbulence. The difference between the fit and the stored array of data yields the phase errors, i.e.,

$$OPD_i = ORD_i - f(x_i, y_i) \tag{10}$$

where OPD_i is the optical path difference at point i in the matrix, and ORD is the fringe order at point i. The RMS phase aberration due to turbulence is then computed from the RMS value of OPD. Using this analysis we can thus effectively compute the random phase aberration due to turbulence as separated from any deterministic aberration.

As mentioned earlier, within each sample area of the interferograms, digital samplings were made at intervals comparable to the fringe spacings, which were about 2 mm in our experiments. Since the turbulent macroscale varies with streamwise distance, the sampling interval can be larger or smaller than the turbulence scale size. However, in calculating the RMS phase aberration, the ratio of the sampling interval to the turbulence scale size has no effect on the accuracy of the results. This is so since the RMS phase aberration calculated here can be considered as obtained by ensemble averaging.[5] In section 4.0 it is shown that the values of α related to the RMS phase aberration obtained in these experiments, throughout the shear layers, are in agreement with values obtained in all previous turbulent measurements in shear flows. The agreement confirms the adequacy of the sampling technique used here.

The largest uncertainty in the RMS phase aberration results is due to reading of the interferometric fringes, which were of finite thickness. The thickness, as observed in the interferogram, is about 0.3 of the fringe spacings. If the reading errors are random about the center of the fringe an estimated error in phase aberration is given as

$$\epsilon \cong \pm \frac{0.3}{2\sqrt{2}} = \pm 0.10 \text{ fringe spacing.}$$

Scatter in actual readings, as presented in the next section, is, however, only about one half of this estimate, since care was exercised in locating the center of each fringe.

5. Bendat, J.S. and Piersol, A.G., Random Data: Analysis and Measurement Procedures, J. Wiley & Sons, p. 68, 87, 288, (1971).

4.0 TEST DATA AND RESULTS

4.1 VERIFICATION OF THEORY

The square root of the beam degradation of the RMS value of the phase aberation as given earlier is

$$\psi' = \sqrt{2}\, k\, \Delta n\, \alpha \sqrt{L\ell} \tag{11}$$

Here we use ψ' to denote the RMS value of the phase aberration; k is the wave number equal to $2\pi/\lambda$. Since

$$\ell \simeq L/4 \tag{12}$$

as measured for many shear and wake flows[6] we get

$$\psi' \simeq \frac{1}{\sqrt{2}}\, k\, \Delta n\, \alpha L \tag{13}$$

To test the analytical expression above, we have measured ψ' for single mixing layers, with Δn varying from 0 to 2.45×10^{-4}. To avoid large velocity nonuniformity in the free stream, a 150 mesh screen was positioned over the orifice plate (see Section 4.3). Interferograms for phase aberration studies were 5.08 cm wide, and 20 cm high in the stream-wise direction. Interferograms for mixing layer growth studies were 7.1 cm wide and 20 cm high. Figures 8a through 8f are typical interferograms obtained.

For each phase aberration interferogram, a middle portion was digitized and processed to obtain the magnitude of phase aberration. The processed area was 7.2 cm high and 4.1 cm wide and the lower edge of the area was 7.2 cm downstream of the edge of the splitter plate. Along the length of this area, the mixing layer thickness increased by about 50%. The average thickness of layers studied varied from 0.6 to 0.9 cm. The experimental results of 14 layers studied are listed in Table 1. Typical phase aberration contours of the analyzed interferograms are shown in Figures 9a and 9b. These show the magnitude of the phase aberration normalized to 2π for the interferometer laser wavelength of 5260 Å. (All other phase aberration data presented in this section are for λ = 5360 Å.) The field of view of the interferograms extends upstream to the edge of the splitter plate, 0.63 cm from the screen surface (see Fig. 3b).

---

6. Batt, R.G., "Turbulent Mixing of Passive and Chemically Reacting Species in a Low-Speed Shear Layer," J.F.M., Vol. 82, 1977, pp. 53-95.

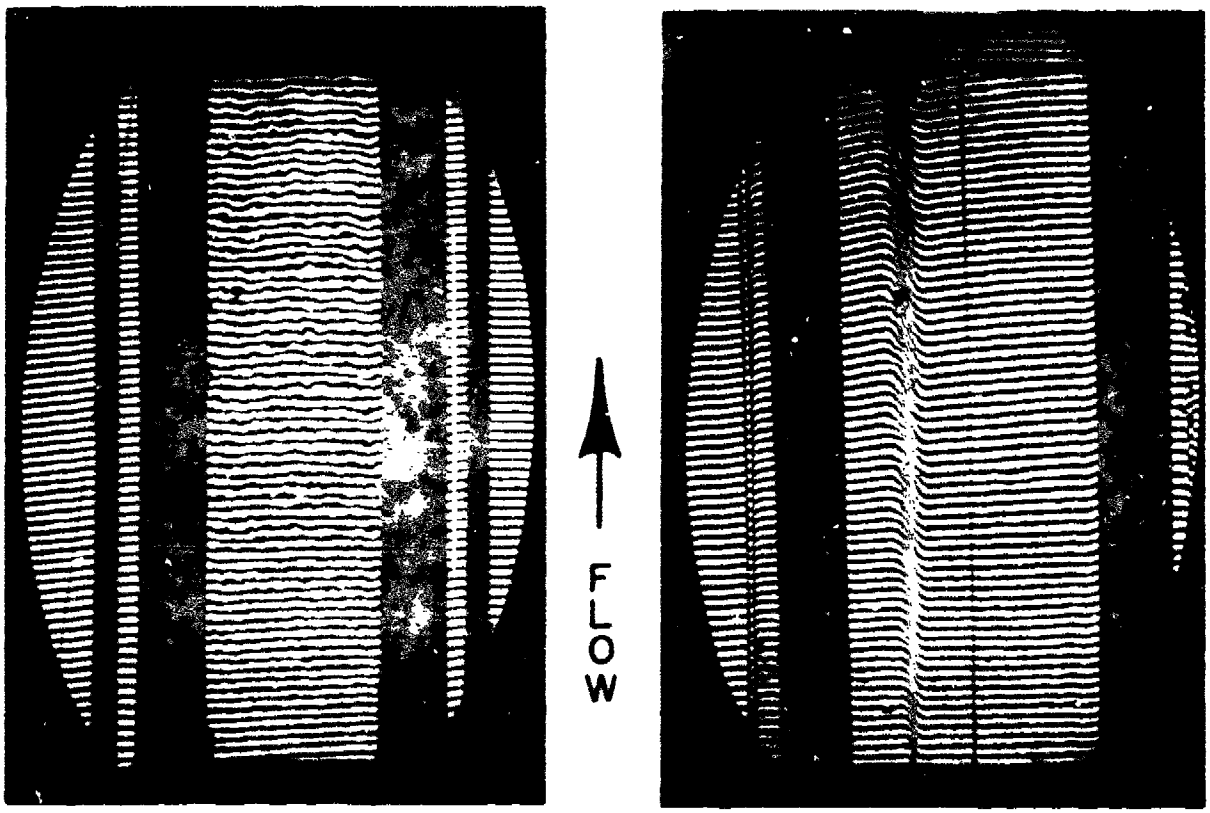

Figure 8a/b Beam Degradation (a), Viewed Perpendicular to Mixing Plane, and Mixing Layer Growth (b), Viewed Parallel to Mixing Plane, for $\bar{n} = 6.2 \times 10^{-5}$, $P_{N_2} = 30$ psig, $P_M = 28$ psig and $\lambda = 5260$ Å (See Table 1)

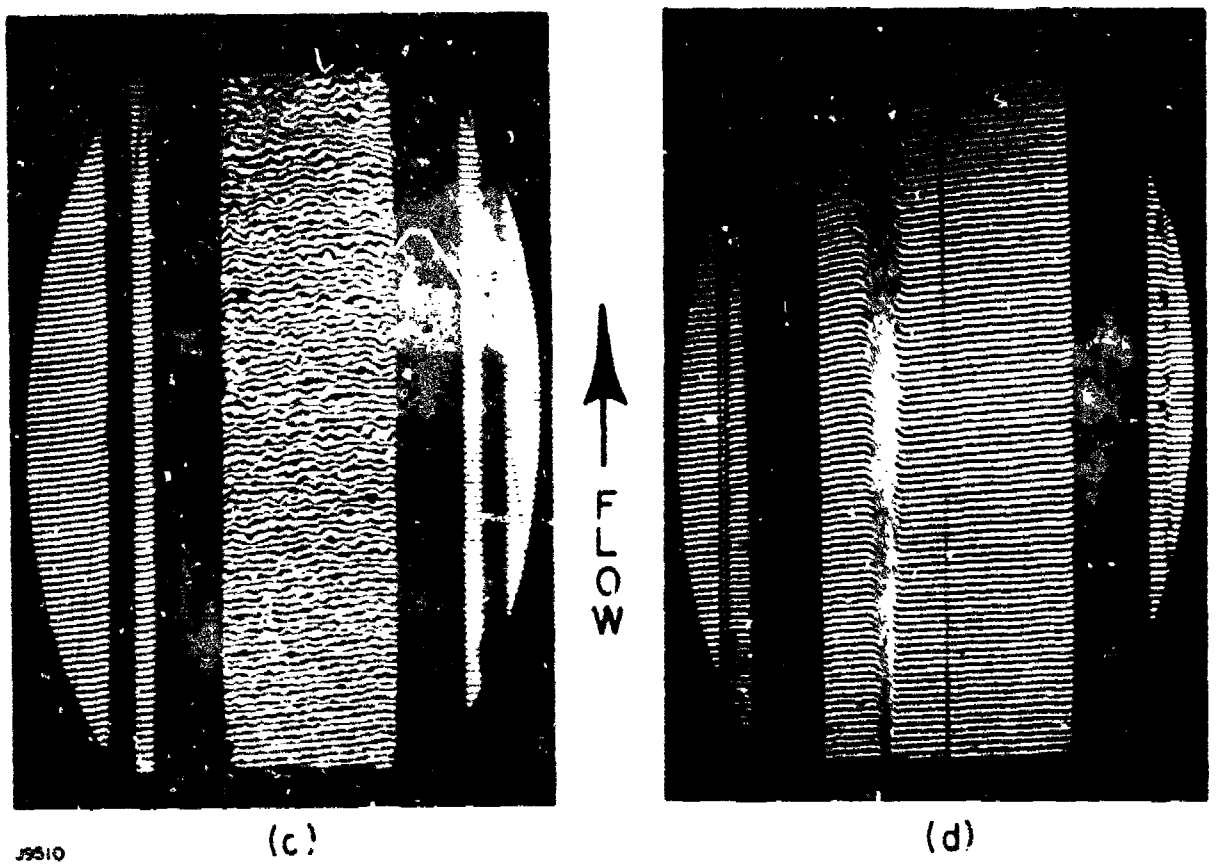

Figure 8c/d Beam Degradation (c) and Mixing Layer Growth (d) for $\delta n = 16.0 \times 10^{-5}$, $P_{N_2} = 30$ psig, $P_M = 19.5$ psig and $\lambda = 5260$ Å (See Table 1)

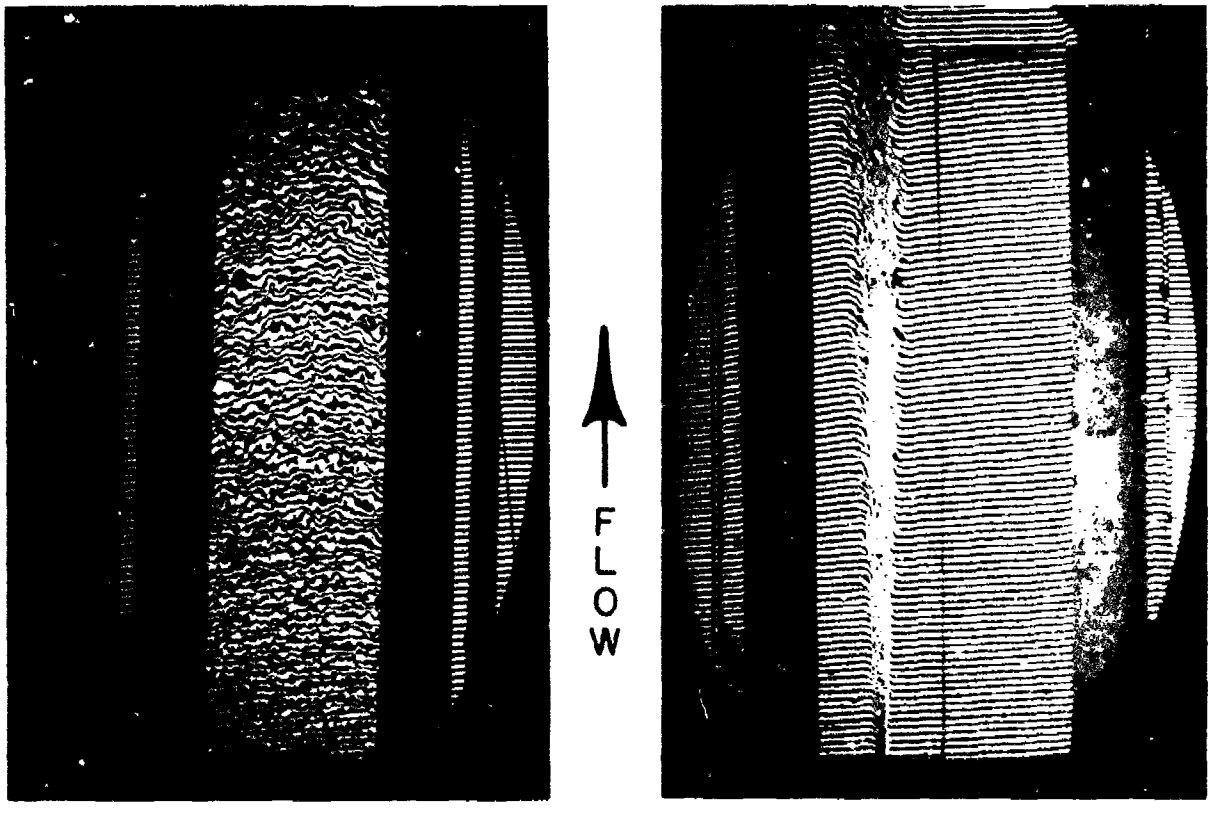

Figure 8e/f Beam Degradation (e) and Mixing Layer Growth (f) for $\Delta n = 24.5 \times 10^{-5}$, $P_{N_2} = 30$ psig, $P_M = 7$ psig and $\lambda = 5260$ Å (See Table 1)

TABLE 1

DEPENDENCE OF PHASE ABERRATION ON Δn*

X_{He}	$\Delta n \times 10^5$	$\psi/2\pi$	L (cm)	$\psi'/2\pi L$ (cm^{-1})	P_M (psig)	V_M (m/s)
0.25	6.2	0.12	0.60	0.20	28.0	32.0
0.25	6.2	0.10	0.60	0.16	28.0	32.0
0.29	7.2	0.13	0.63	0.21	20.0	25.7
0.29	7.2	0.14	0.65	0.22	25.0	29.4
0.38	9.3	0.17	0.68	0.26	29.0	35.1
0.38	9.3	0.20	0.68	0.29	29.0	35.1
0.42	10.3	0.15	0.60	0.25	25.0	31.9
0.42	10.3	0.16	0.60	0.27	25.0	31.9
0.65	16.0	0.26	0.65	0.39	19.5	33.8
0.68	16.6	0.35	0.90	0.39	40.0	55.7
0.76	18.6	0.30	0.73	0.41	16.0	34.5
0.80	19.6	0.36	0.73	0.49	16.0	36.3
1.0	24.5	0.36	0.70	0.52	7.0	35.5
1.0	24.5	0.44	0.75	0.59	7.0	35.5

*Nitrogen stream at 28.5 m/s (plenum pressure 30 psig); V_M is the gas mixture velocity, P_M the gas mixture plenum pressure and λ = 5260 Å

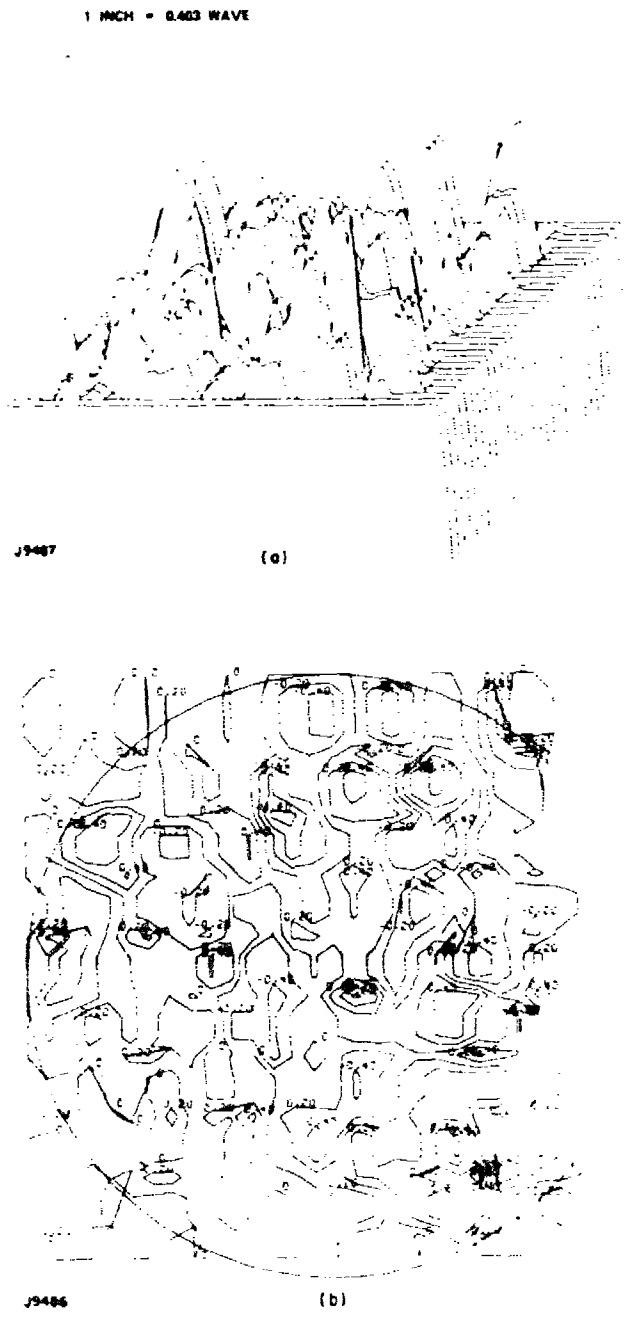

Figure 9 Phase Aberration Isometric (a) and Iso-Contour (b) Maps for $\Delta n = 18.6 \times 10^{-5}$, $P_{N_2} = 30$ psig, $P_M = 16$ psig and $\lambda = 5260$ Å (See Table 1)

The functional dependence of ψ' on Δn can be seen in Figure 10. Here the values of phase aberration per unit mixing layer thickness $\psi'/2\pi L$ are given. We can see that $\psi'/2\pi L$ increases linearly with Δn. The solid line plots the theoretical values of $\psi'/2\pi L$ computed from Eq. (13) with $\alpha = 18\%$. This value of α is in accordance with measured values obtained in a large number of shear and wake flows.[6] Agreement between experimental and analytical results can be seen.

To study how ψ' varied with the streamwise distance x, several interferograms were divided into five contiguous portions and analyzed; each portion was a rectangle 4 cm high and 4.5 cm wide. The results are listed in Table 2 and plotted in Figure 11. The values of L and x were measured at the center of each portion. The results were obtained for two values of Δn, 2.45×10^{-4} and 1.86×10^{-4}. (For the ABEL laser, $\Delta n = 1.82 \times 10^{-4}$). It can be seen that L and ψ' had finite values at $x = 0$ and then increased linearly with x. (See the following subsection for further discussions on the finite values of L at $x = 0$). The solid lines for ψ' present its theoretical values based on the measured values of L and with $\alpha = 14\%$. This value of α is slightly lower than that obtained from Figure 10, but both are in agreement with measured values in other mixing layer experiments.[6]

In summary, the data obtained in this series of experiments indicate that ψ' is proportional to Δn and L as predicted by Eq. (2) or Eq. (13).

4.2 EFFECT OF VELOCITY SHEAR

The growth of the mixing layer thickness depends both on the intensity and macroscale of the turbulence in the free stream as well as the velocity difference between the two streams. Brown and Roshko[4] also reported a slight dependence of the growth rate on the ratio of the densities. In this series of experiments, we studied the growth rate of the mixing layer between nitrogen and four different gas mixtures. A 150-mesh screen was positioned over the orifice plate to produce uniform free-stream velocity (see Section 4.3). In each stream the turbulence intensity was 2% at 1 cm downstream of the screen.

Typical interferogram results are shown in Figures 12a through 12c. It can be seen that L grows with downstream distance x and the growth rate increases with higher shear. At $x = 0$, the layer thickness L is about 1.5 mm for all mixing layers studied. The virtual origin of the layer where $L = 0$ is thus extrapolated to be several centimeters upstream of the edge of the splitter plate. The layer thickness is measured with the method discussed in Section 3.1.

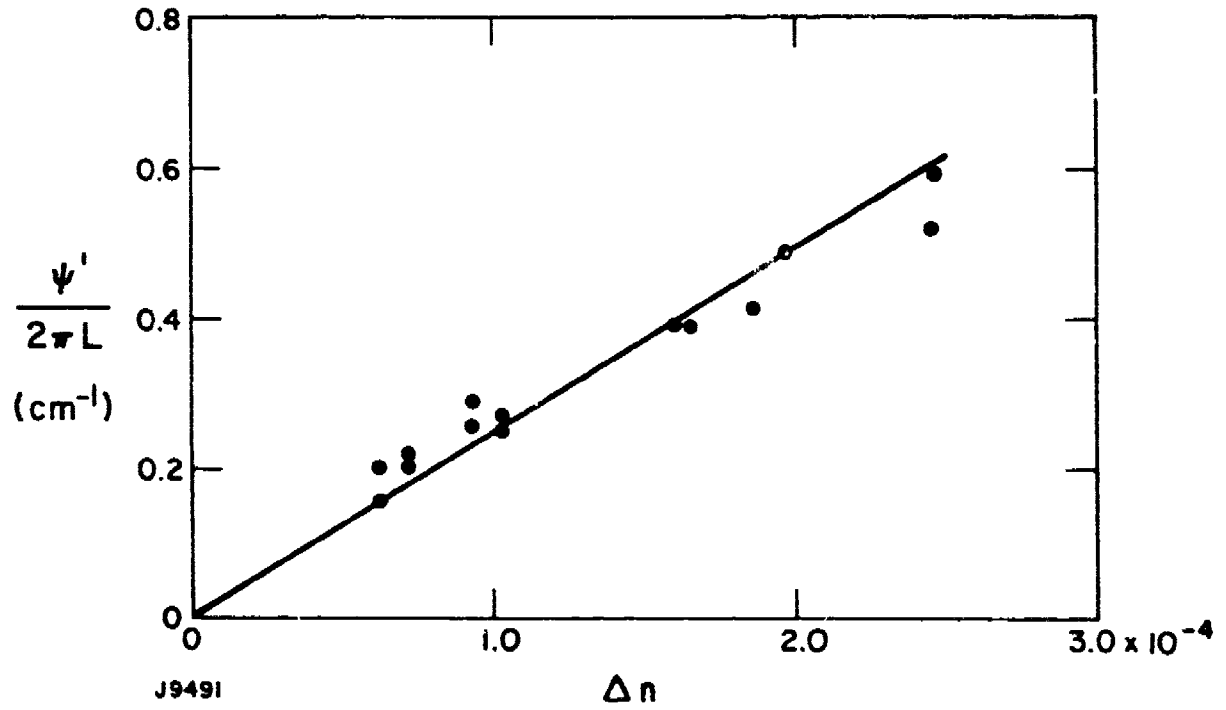

Figure 10 Phase Aberration as a Function of Δn; λ = 5260 Å

TABLE 2

PHASE ABERRATION ALONG STREAMWISE DISTANCE*

x_{He}	$\Delta\rho$ $\times 10^{5}$	P_M (psiq)	V_M (m/s)	P_{N_2} (psiq)	V_{N_2} (m/s)	x (cm)	L (cm)	$\psi'/2\pi$ Meas'm't 1	$\psi'/2\pi$ Meas'm't 2
1.0	24.5	7.0	35.5	30.0	28.5	2.0	0.36	0.17	0.23
						6.0	0.58	0.28	0.28
						10.0	0.80	0.35	0.36
						14.0	1.00	0.42	0.41
						18.0	1.15	0.44	0.48
0.76	18.6	16.0	36.5	30.0	28.5	2.0	0.40	0.17	0.16
						6.0	0.55	0.22	0.23
						10.0	0.90	0.26	0.24
						14.0	1.00	0.30	0.33
						18.0	1.15	0.39	0.38

*λ = 5260 Å

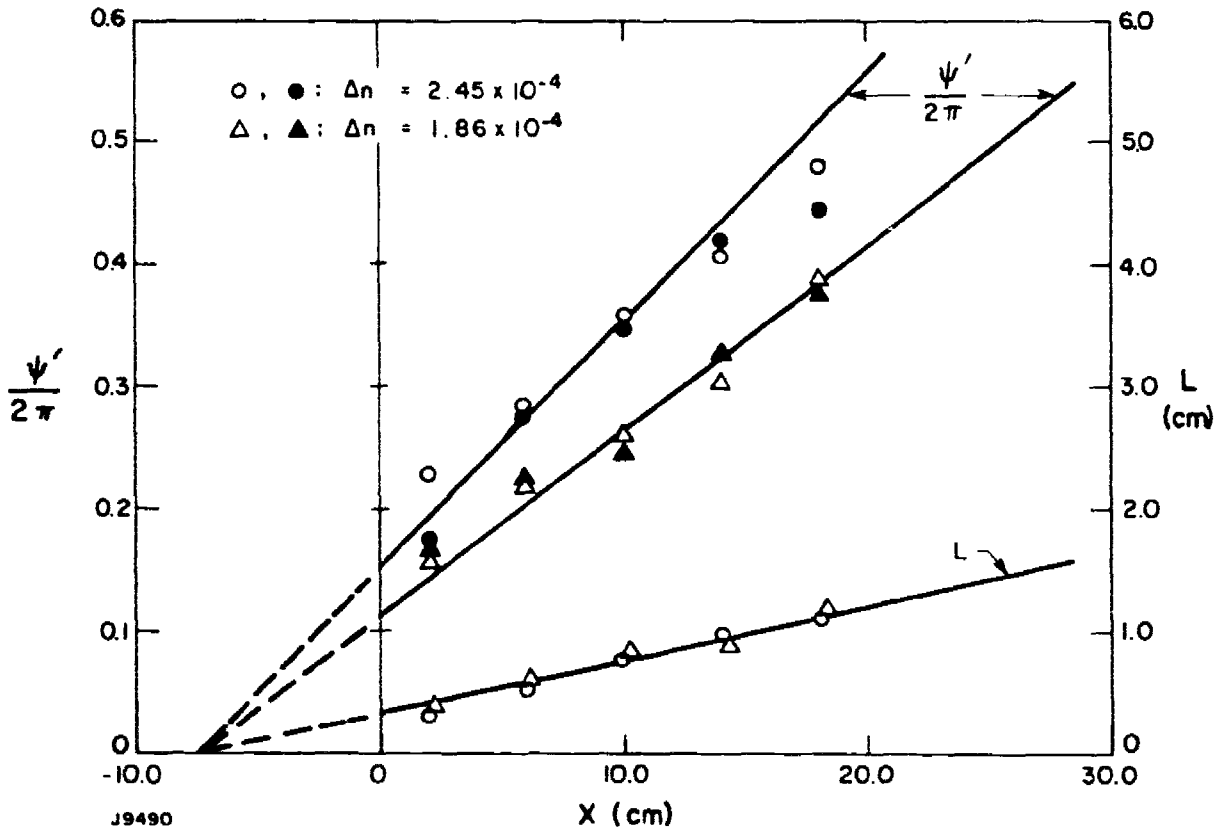

Figure 11 Evolution of Phase Aberration and Mixing Layer Thickness Along Stream-wise Direction; λ = 5260 Å

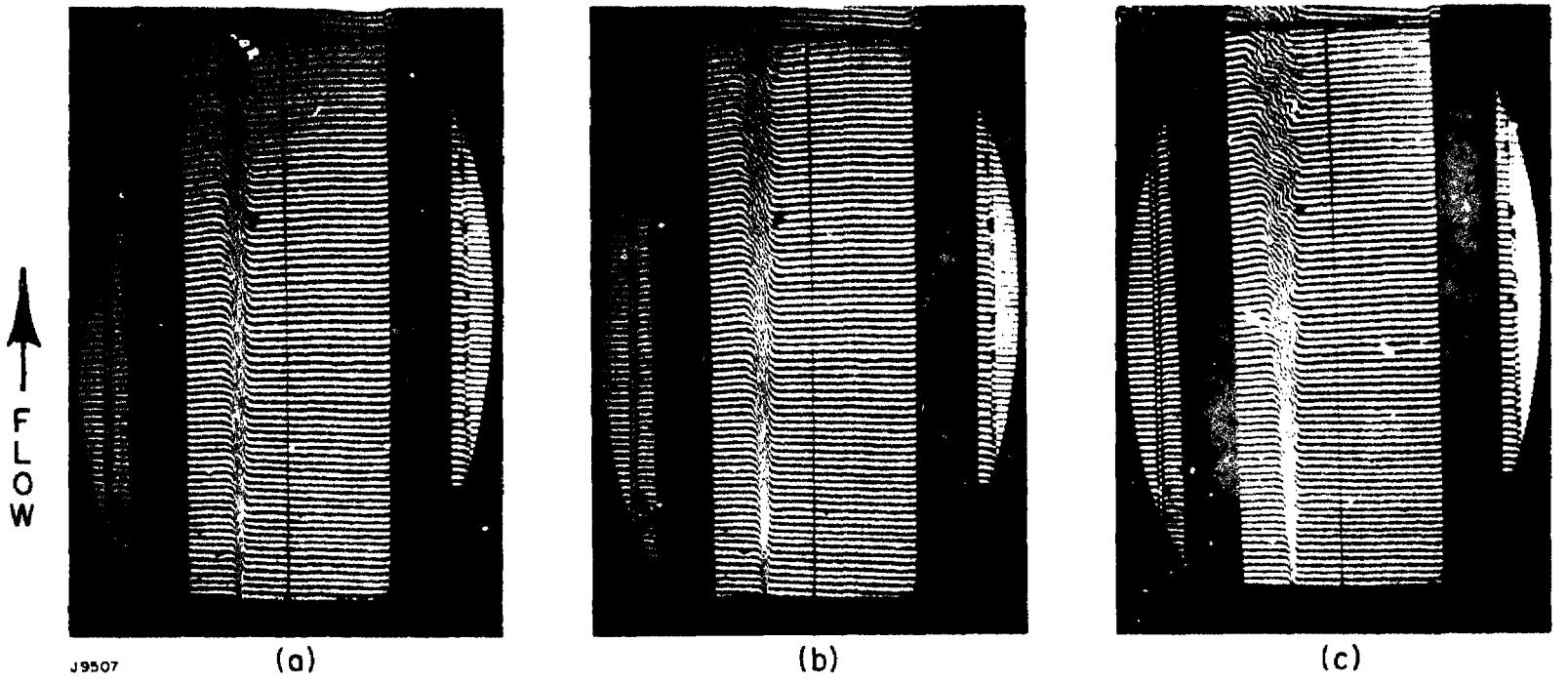

Figure 12 Effect of Shear on Mixing Layer Growth for $\Delta n = 7.2 \times 10^{-5}$, $\lambda = 5260$ Å and (a) R = 0.07, (b) R = -0.13 and (c) R = -0.21 (See Table 3)

Sabine[7] and Abramovich[8] suggested that the growth rate of a shear layer thickness is a function of the ratio

$$R = \frac{U_1 - U_2}{U_1 + U_2} \tag{14}$$

where subscript "1" denotes the lighter gas and "2" the heavier gas. In Figure 13 we thus plot the growth rate,

$$L' = dL/dx$$

against the shear ratio, R.

The data, which cover the region of practical interest, $|R| \lesssim 0.4$, are also presented in Table 3. L' can be observed to increase with the absolute value of R. For small values of $|R|$ (< 0.1) where shear layers in aerowindows are likely to operate the growth rate is about 5%. Measurements were taken for four density ratios of 1.33, 2.40, 3.18 and 7.0 (with respective values of Δn of 0.72×10^{-4}, 1.66×10^{-4}, 1.96×10^{-4} and 2.45×10^{-4}), but no marked effect of the density on growth rate was observed.

In Figure 13 the shear flow data in this experiment are presented together with data of Brown and Roshko.[4] Their data show that for values of R higher than 0.4, the growth rate increased linearly with R; a more marked effect of density on growth rate was also reported. Our data in the region of interest of $|R| < 0.4$ appear to converge to the lowest of the growth rates reported by Brown and Roshko. It should be noted, however, that the Brown and Roshko data were obtained by a somewhat subjective visual observation of the shadowgraphs.

The Brown and Roshko coherent structures could also be observed in our experiments (see Figure 12c). These structures become much more pronounced for $|R| > 0.3$. It is, thus advisable for aerowindow application to use shear layers with $|R| < 0.1$.

---

7. Sabin, C.M., "An Analytical and Experimental Study of the Plane, Incompressible, Turbulent Free-Shear Layer with Arbitrary Velocity Ratio and Pressure Gradient," Trans. ASME. D. 87, 1965, pp. 421.

8. Abramovich, G.N., The Theory of Turbulent Jets, M.I.T. Press 1963.

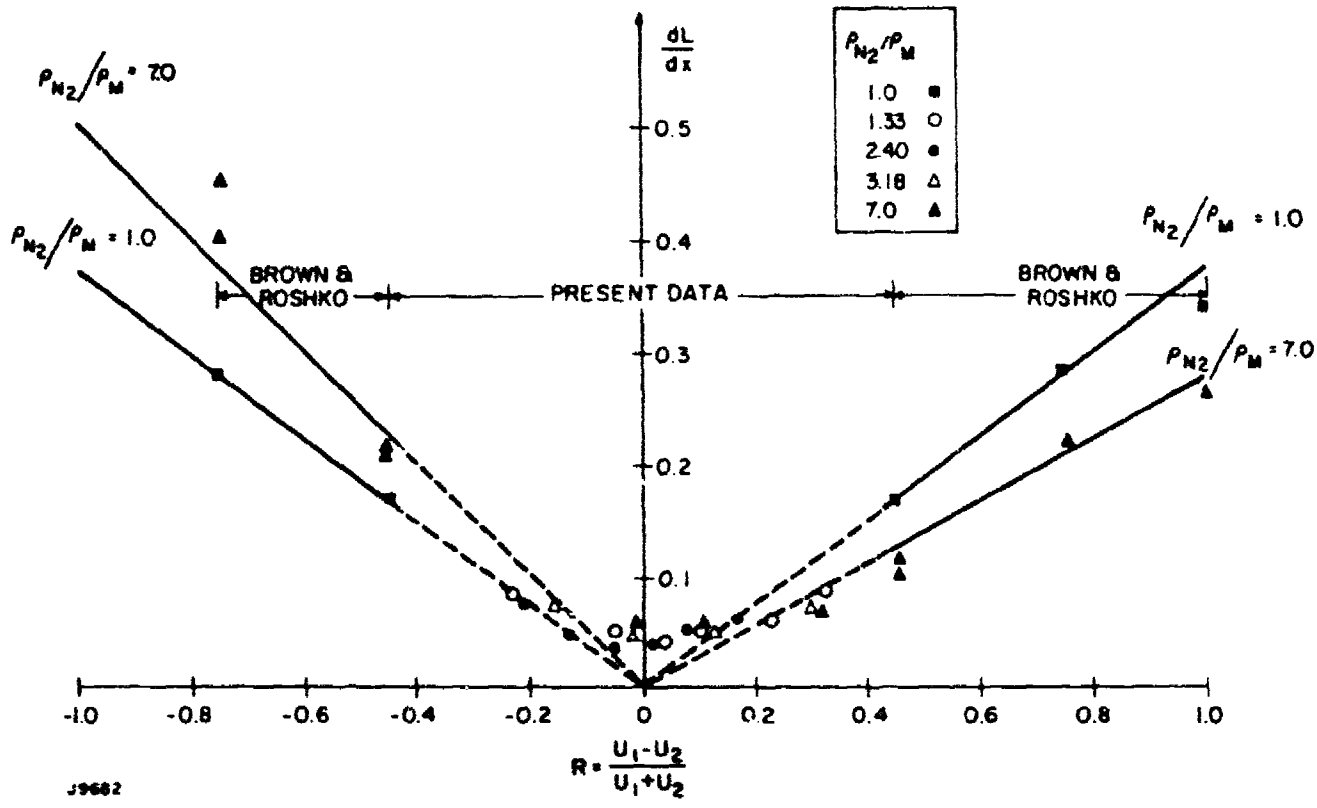

Figure 13 Effect of Velocity Shear on Mixing Layer Growth Rate; Lines Through Brown and Roshko Data Points (Ref. 4) are Sabin and Abramovich (Refs. 7 and 8) Semiempirical Theory for Large |R|

TABLE 3

EFFECT OF SHEAR ON MIXING LAYER GROWTH AND BEAM DEGRADATION*

ρ_{N_2}/ρ_M	n × 10[illegible]	P_M (psig)	V_M (m/s)	$\frac{U_1 - U_2}{U_1 + U_2}$	dL/dx	[illegible]	[illegible] × 10⁻⁴
1.33	7.2	10	18.6	-0.21	[illegible]	0.19	[illegible]
		15	22.0	-0.11	0.050	0.14	[illegible]
		20	25.7	-0.05	0.040	0.11	[illegible]
		25	29.4	0.01	0.045	0.14	[illegible]
		30	33.4	0.03	0.055	0.12	[illegible]
		40	41.0	0.17	0.063	—	—
2.1[illegible]	16.6	5	17.9	-0.21	0.085	0.34	[illegible]
		10	25.6	-0.05	0.055	0.32	[illegible]
		15	30.4	0.04	0.045	0.25	[illegible]
		20	35.2	0.10	0.055	0.28	[illegible]
		20	35.2	0.10	0.055	0.27	[illegible]
		30	45.6	0.24	0.065	0.34	[illegible]
		40	55.7	0.32	0.085	0.35	[illegible]
		40	[illegible]	0.32	0.085	0.44	[illegible]
[illegible]	29.4	5	[illegible]	-0.16	0.025	0.40	[illegible]
		5	20.7	-0.16	0.025	0.36	[illegible]
		10	29.6	0.02	[illegible]	0.34	[illegible]
		15	36.2	0.12	[illegible]	0.30	[illegible]
		20	40.9	0.18	—	0.36	[illegible]
		30	[illegible]	0.30	0.075	0.38	[illegible]
		40	52.[illegible]	0.39	0.075	0.44	[illegible]
[illegible]	24.5	4	28.0	-0.01	0.060		[illegible]
		[illegible]	35.5	0.11	0.063	0.36	[illegible]
		[illegible]	45.5	0.11	0.060	0.42	[illegible]
		[illegible]	54.0	0.11	0.070	0.41	[illegible]

*Nitrogen stream at 28.5 m/s (plenum pressure 30 psig); λ = 5260 Å

The effect of shear on phase aberration is shown in Figure 14. The aberrations were obtained for the rectangular middle portion of the shear layers which was 7.2 cm high, 4.1 cm wide and with its lower edge 7.2 cm downstream of the splitter plate edge. Here, the normalized values of $\psi'/2\pi\,\Delta n$ are plotted against R. For $|R|<0.1$ the normalized pnase aberration is about 0.18×10^4 for $\lambda = 5260$ Å.

4.3 EFFECT OF FLOW PLATE

In this series of experiments, we studied the effect of a screen positioned over the orifice plate on the free-stream velocity as well as the mixing layer growth rate and phase aberration.

The two flow plates are shown in Figures 3a and 3b. The screen used is a 150-mesh screen with 34% open area. The junction between the screen and splitter plate must be carefully made. Various designs for the junction between the screens and splitter plate extension were tried. Figure 15 shows the nonrandom nonuniformity introduced in the mixing layer by one unsuccessful design, illustrated in Figure 16. The design finally decided upon (Figure 17) gave very satisfactory results. The design uses two splitter plate extensions with a fine mesh screen clamped between them. Clamping insures good alignment between the two extensions and introduces minimal flow disturbance near the splitter plate. The wires of the screen are oriented 45° with respect to the splitter plate to avoid formation of large-scale nonuniformities. Flow near the splitter plate was measured by a hot-wire along the extension with the wire positioned 1 mm away from the extension and 3 mm down stream of the screen. Flow uniformity along the splitter plate extension was comparable to that in the free stream. This design was thus used for the experiments done in this test.

The free-stream velocity profiles for the screened and unscreened flow plate are shown in Figure 18. A screen of 150-mesh was used. Quite noticeable differences between the two profiles can be observed. Without a screen, the flow is very nonuniform. The scales of nonuniformity are observed to be several (3 or 4) times as large as the orifice spacing. This is the result of jet coalescence developed in orifice plates with open area ratios of less than about 60%.(9)

---

9. Kuchemann, D. and Sterne, L.H.G., (1964), Progress in Aeronautical Sciences, V5; "The Design of Low Speed Wind Tunnels," p. 12, 13, 28, 29, 30, 31.

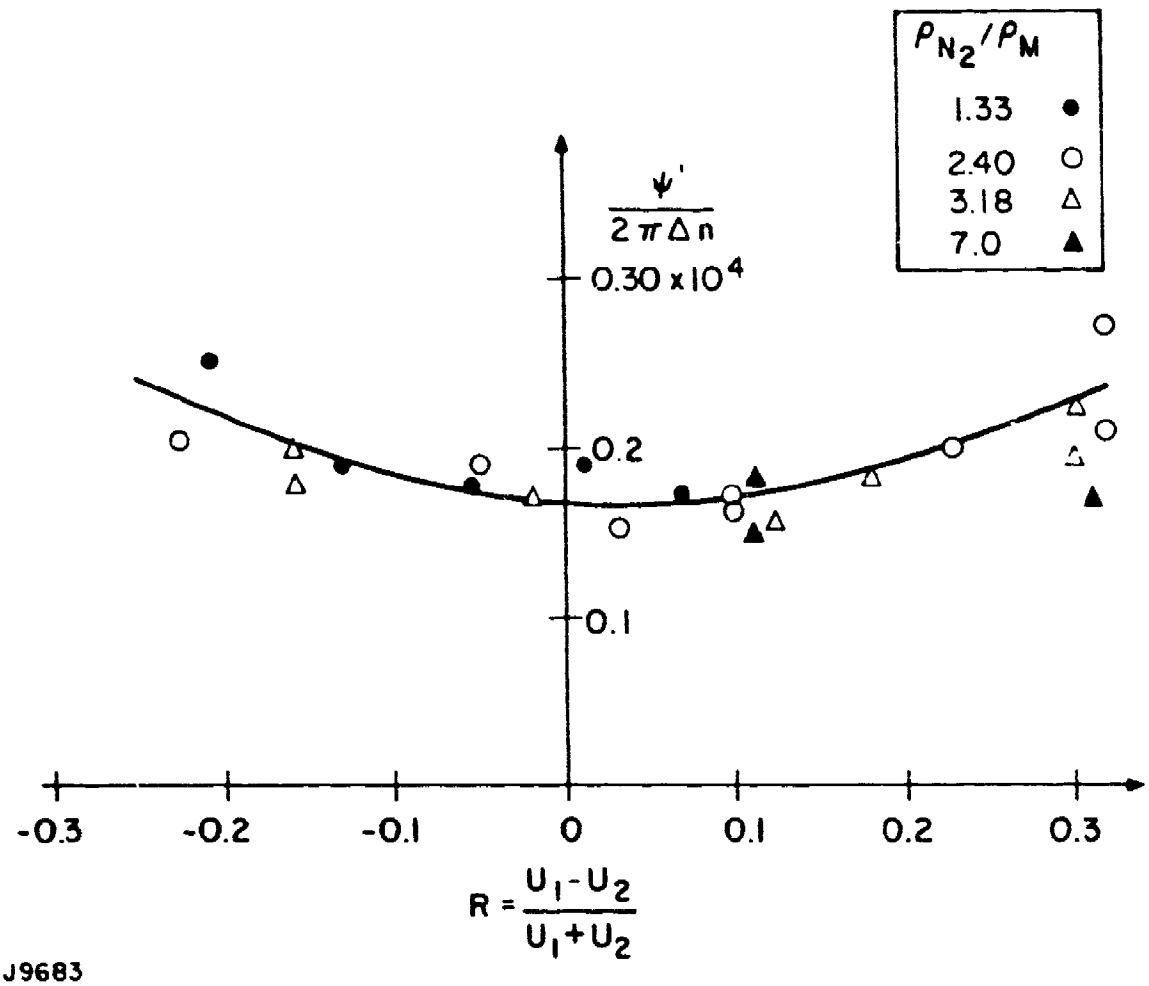

Figure 14 Effect of Shear on Phase Aberration; λ = 5260 Å

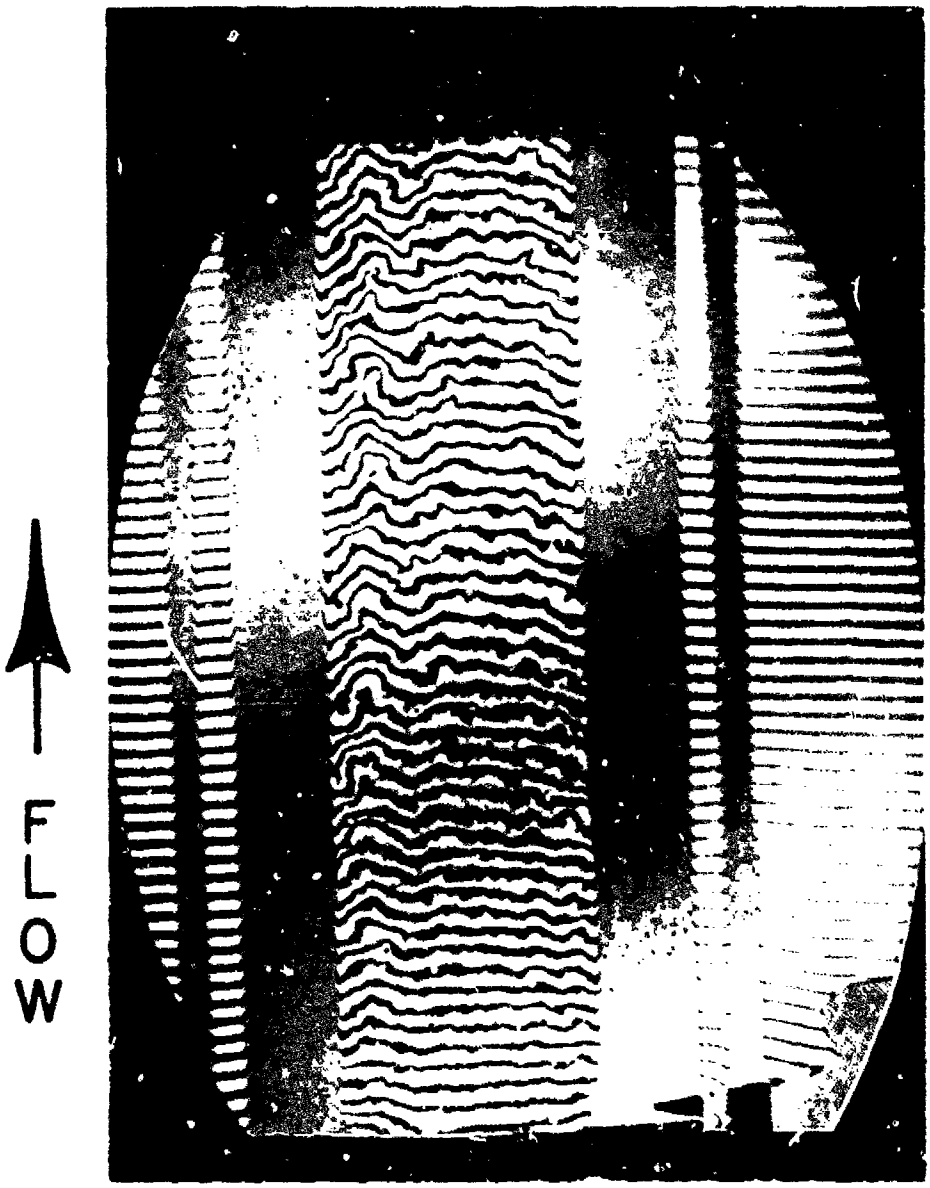

J9506

Figure 15 Non Random, Non-Uniformity Introduced by the Unsuccessful Flow Plate Modification Illustrated in Figure 16; λ = 5260 Å

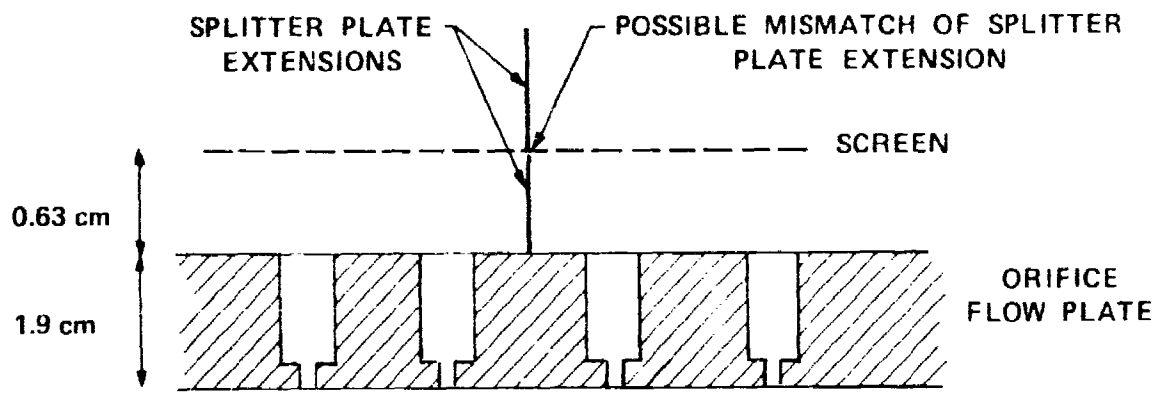

Figure 16 Modified Flow Plate of Unsuccessful Design

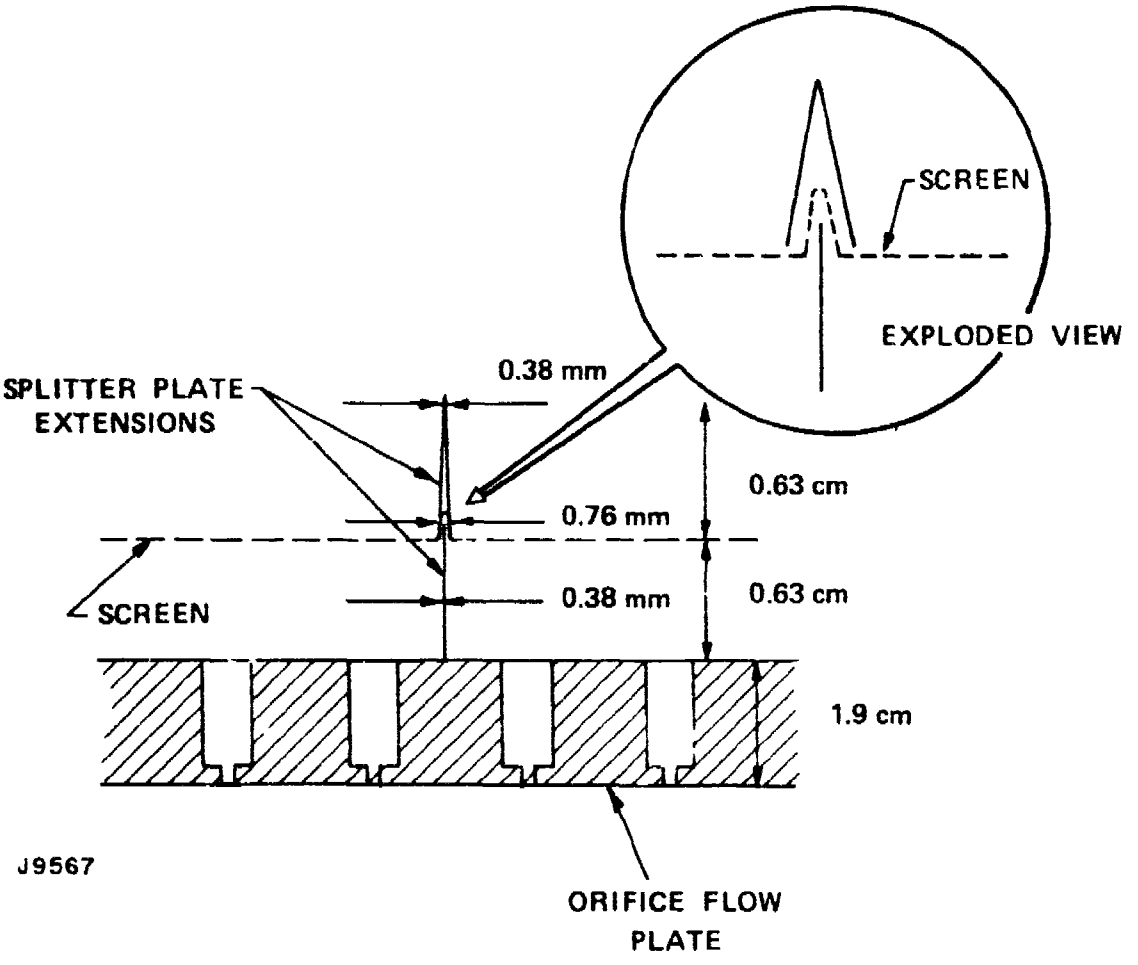

Figure 17 Modified Flow Plate of Successful Design

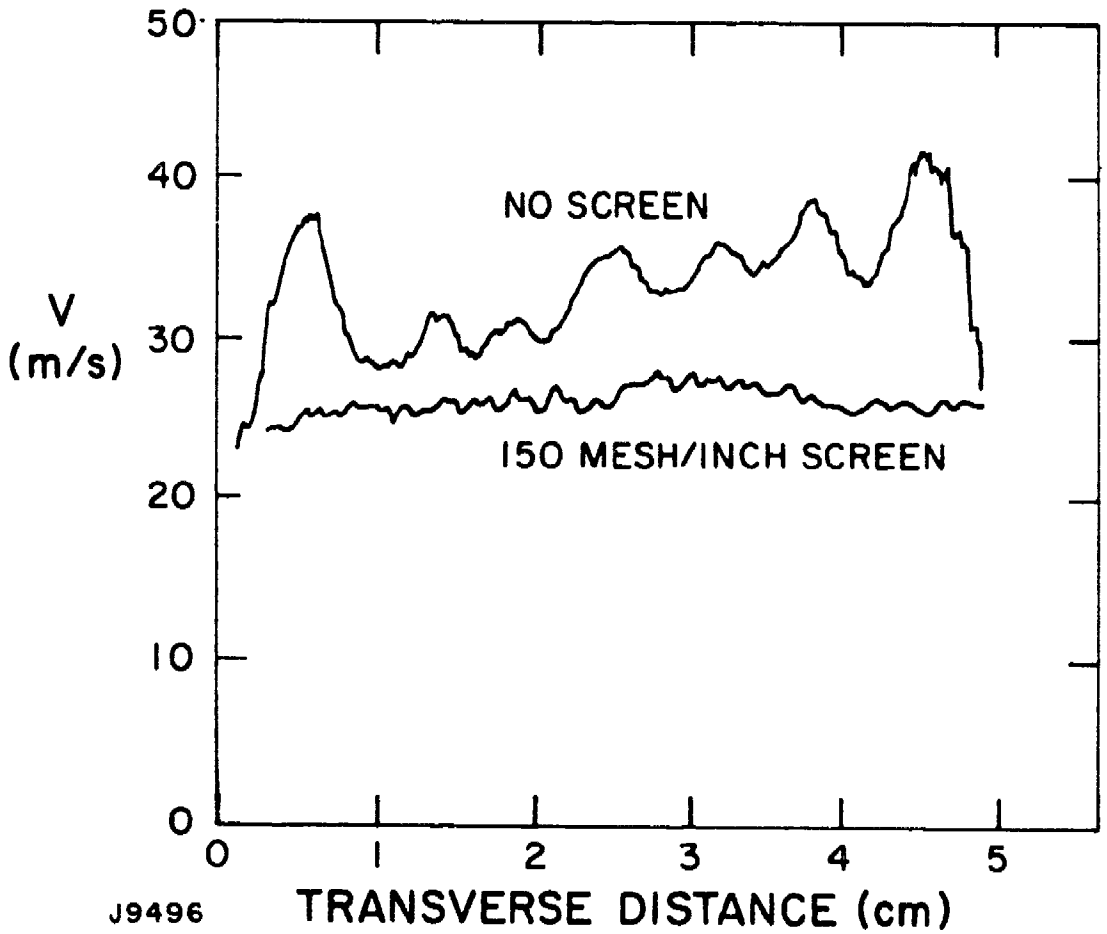

Figure 18 Effect of Screening on Flow Uniformity; Measurements Made 1.27 cm Downstream of Orifice Flow Plate

To obtain uniform flow from the flow plate, it is important that a fine-mesh screen be positioned over the plate so that jets from the plate can be "broken" up. "Jet Breaking" is more pronounced with finer mesh screens which give higher flow resistance. Figure 19 shows the velocity profiles measured for various screens. Screens with mesh number higher than 100 give good uniformity. These finer screens are usually manufactured with an open area ratio <40%, and jet coalescence occurs. The scales of nonuniformity, as observed in Figures 18 and 19, are, however, kept small due to the small mesh size. A mesh size of 150 was chosen to be used in our experiment, as a compromise between strength and effectiveness in smoothing out free-stream velocity.

The effect of the screen on mixing layer growth rate and phase aberration was studied with two values of Δn of 0.62×10^{-4} and 1.03×10^{-4}. The shear ratio, R, of the mixing layers was taken to be about 0.06. It should be noted that, in order to keep farfield beam degradation (due to shear layer turbulence) negligible, $|R|$ should be less than 0.1. As shown in Figures 20a and 20b,* the mixing layer growth rate is much higher for the unscreened flow plate. The growth rate, as well as the phase aberration for the middle portion of the mixing layer (7.2 x 4.1 cm^2 area with the lower edge 7.2 cm from the splitter plate end) are listed in Table 4 and presented in Figure 21; the dotted lines on the plot are theoretical extrapolations based on Eq. (2). For the unscreened plate, the growth rate and aberration are about twice as large as those for the screened flow plate. This means that the beam degradation for the screened flow plate is only about one-fourth of the degradation for the unscreened flow plate. Screening is thus a very good method for reducing beam degradation.

Another advantage of screening is that the phenomena of mixing layer bending and deflection observed for the unscreened flow plate, does not occur. This phenomena as reported earlier[2] occurs for the unscreened flow plate when there is an appreciable difference between the pressures of the two plenum chambers upstream of the plate. For the screened plate, similar pressure differences in the plenums do not give rise to noticeable mixing layer bending. (See, for example, the mixing layer in Figure 8f where the pressures in the two plenums are 7 psig and 30 psig.) For the unscreened flow plate the mixing layer bending toward the gas stream with high plenum pressure was most severe within a few centimeters downstream of the flow plate and became unnoticeable further downstream.[2] The apparent reason for the bending is that the gas stream with higher plenum pressure has a higher kinetic energy as shown in Appendix B; the gas stream with higher kinetic energy will create a negative static pressure differential and "pull" the mixing layer toward its side. This "ejector pump effect" is most severe when the difference between

*The field of view in Figure 20a, for the screened flow plate, extends upstream to the edge of the splitter plate, 0.63 cm from the screen; the field of view in Figure 20b, for the unscreened flow plate, extends upstream to the flow plate.

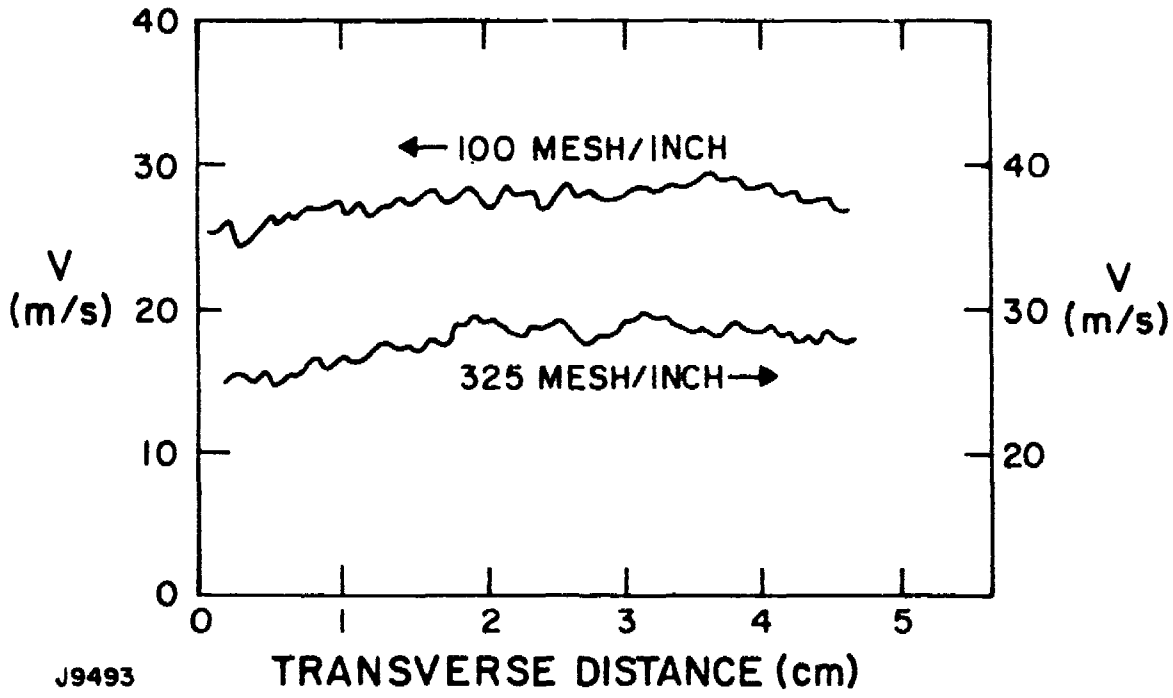

Figure 19 Effect of Mesh Size on Flow Uniformity; Measurements Made 1.27 cm Downstream of Orifice Plate

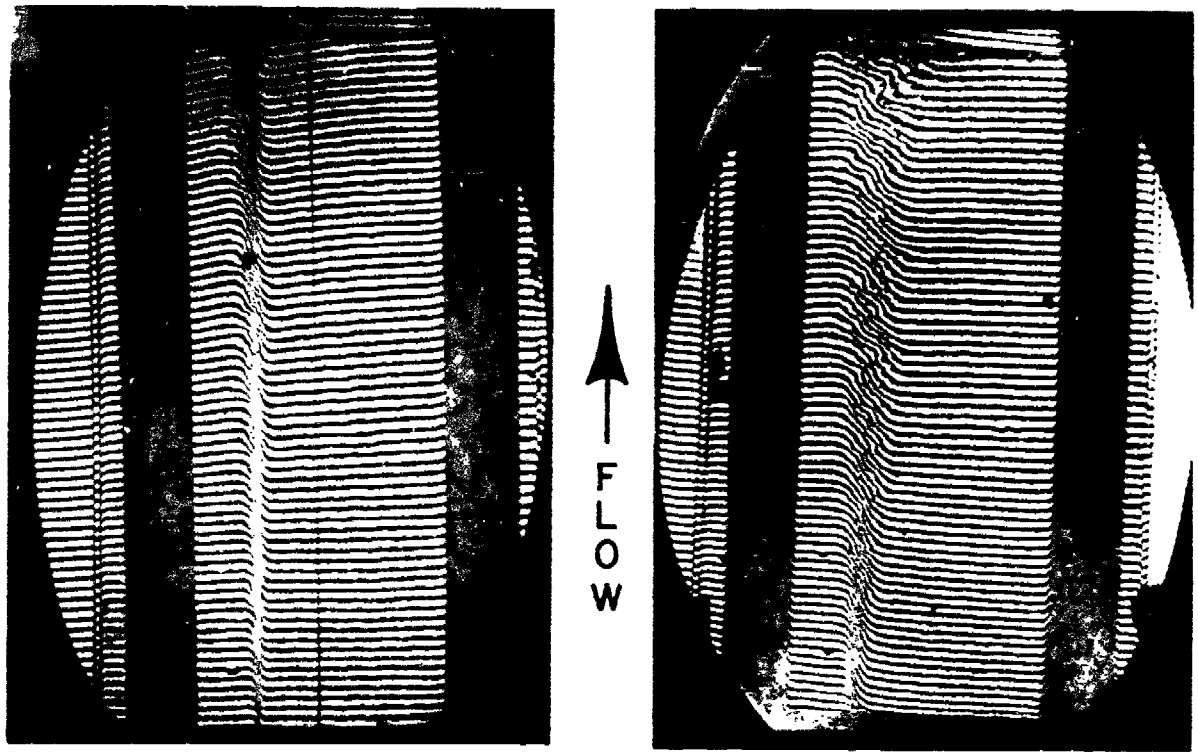

Figure 20 Effect of Screening on Mixing Layer Growth for $\Delta n = 6.2 \times 10^{-5}$ and $\lambda = 5260$ Å (see Table 4) with 150 Mesh/Inch Screen (a) and Without Screen (b)

TABLE 4

EFFECT OF SCREENING ON MIXING LAYER GROWTH AND PHASE ABERRATION*

$\Delta n \times 10^5$	Flow Plate	P_{N_2} (psiq)	P_M (psiq)	V_{N_2} (m/s)	V_M (m/s)	R	$\frac{dL}{dx}$	L (cm)	$\phi'/2\pi$
6.2	Unscreened	24.0	23.0	28.3	32.2	0.064	0.100	1.30	0.20 0.24
6.2	Screened	30.0	28.0	28.5	32.0	0.058	0.045	0.60	0.10 0.12
10.3	Unscreened	24.0	20.0	28.3	32.1	0.063	0.090	1.40	0.31 0.29
10.3	Screened	30.0	25.0	28.5	32.0	0.058	0.045	0.60	0.15 0.16

*λ = 5260 Å

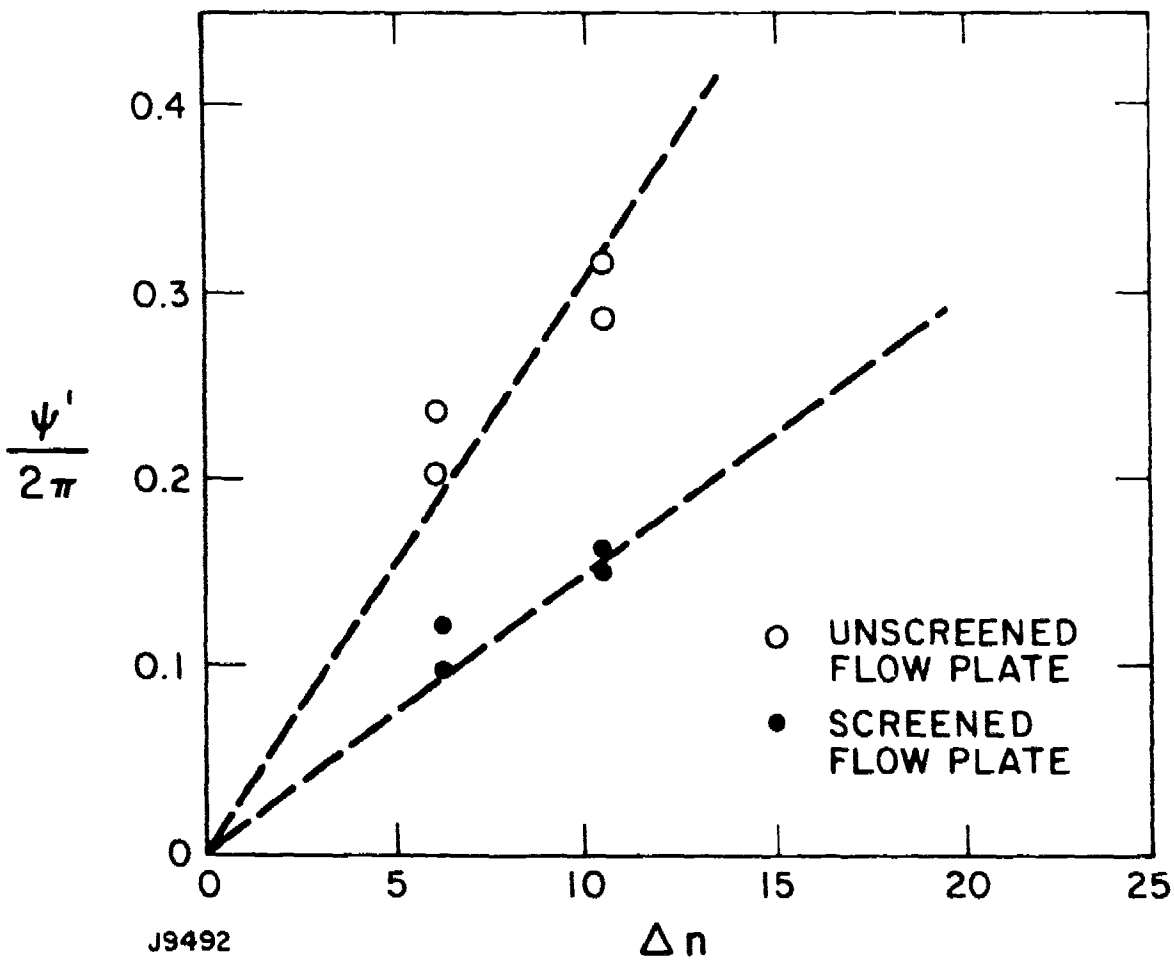

Figure 21 Phase Aberration for Screened and Unscreened Flow Plates and λ = 5260 Å; Shear Ratio R ≅ 0.06

the kinetic energies, and thus the static pressures, of the two streams is highest. For the unscreened flow plate this is the region near the flow plate where jets from the orifices have not yet merged to form a uniform flow. As the orifice plate has an open area ratio of 40.8%, the kinetic energies of the gases, and consequently their difference, in the jetting region is six times higher than those in the uniform flow. The modified flow plate with a fine-mesh screen over the orifice plate has effectively eliminated this jetting region above the screen and thus reduced mixing layer bending to unnoticeable levels.

4.4 EFFECT OF EXPOSING ONE FREE STREAM TO A STAGNANT REGION

As shown in Figure 1, the end flow in the ABEL laser is exposed to a stagnant region which is connected to the aero-window. To study the effect of this stagnant region on the mixing layer, experiments were performed in the flow setup shown in Figure 2 with nitrogen and helium flowing from the two plenum chambers. Experiments were performed under unexposed and exposed conditions. Under the unexposed condition both streams were confined by the chimney walls. Under the exposed condition the nitrogen stream was exposed to the stagnant region and the helium stream confined by the chimney wall; the stagnant region was 5.3 cm away from the mixing layer, and its height h_e was varied from 10 cm to 18 cm.

Interferometer results are shown in Figures 22 and 23. Inspection reveals that the mixing layers in the exposed condition were not markedly different than those under unexposed conditions. No instability, such as wavering of the layers was observed. Quantitative comparisons of the phase aberration are presented in Table 5. The results for layers under both conditions are roughly equal within experimental error.

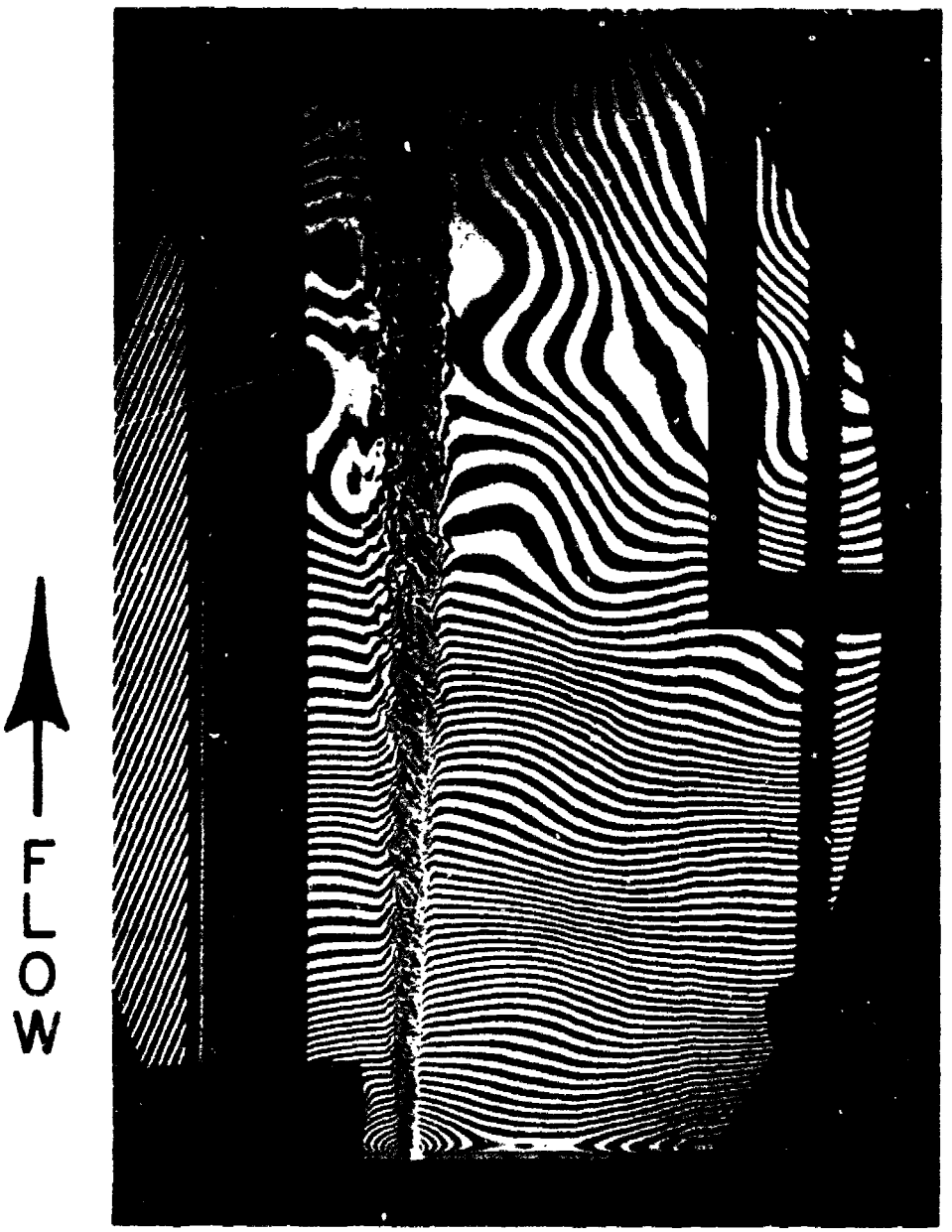

J9505

Figure 22 Mixing Layer Growth with One Stream Open to a Stagnant Region for $\Delta n = 24.5 \times 10^{-5}$, $h_e = 10$ cm, $P_{N_2} = 30$ psig, $P_M = 7$ psig and $\lambda = 5260$ Å (Compare with Figure 8f). The large-scale distortion is due to poor optical quality Plexiglas in the interferometer beam path (other interferograms were taken through a high optical quality quartz window)

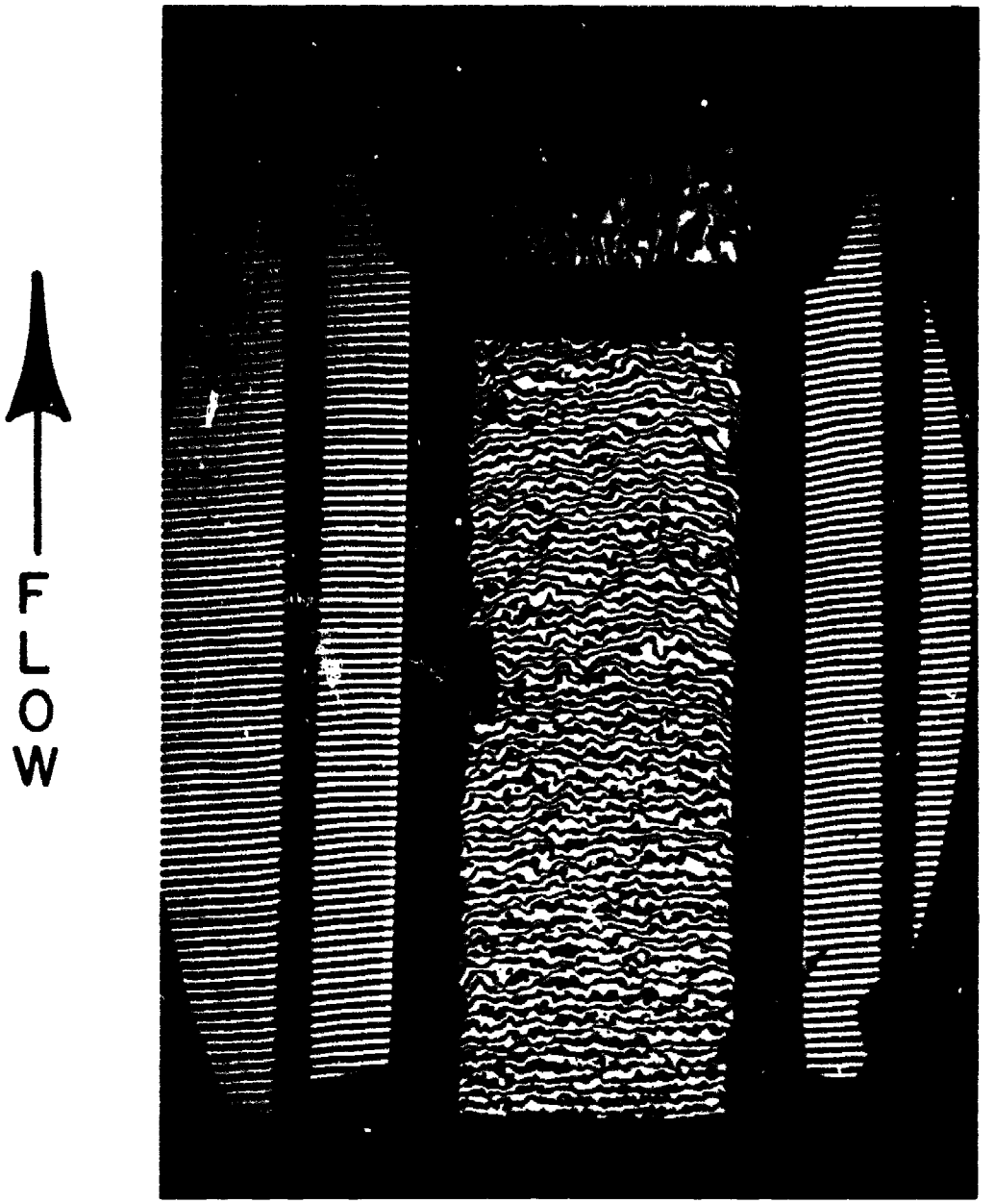

J9767

Figure 23 Beam Degradation with One Stream Open to a Stagnant Region for $\Delta n = 24.5 \times 10^{-5}$, $h_e = 15$ cm, $P_{N_2} = 30$ psig, $P_M = 7$ psig and $\lambda = 5260$ Å (Compare with Figure 8e)

TABLE 5

PHASE ABERRATION $\psi'/2\pi$ FOR DIFFERENT VALUES OF h_e FOR MIXING LAYERS BETWEEN He AND N_2 FLOWING AT 35.5 M/S AND 28.5 M/S RESPECTIVELY*

x (cm) \ h_e (cm)	No Exposure	10.0	15.0	18.0
6.0	0.28	0.28 0.32	———	———
10.8	0.36 0.44	——— ———	0.38 0.43	0.40 0.46

*Values of aberration were obtained from analyzing rectangular areas 4.5 cm wide and 7.2 cm high; x is the streamwise distance of the center of each area; λ = 5260 Å

5.0 SUMMARY AND CONCLUSIONS

The following conclusions can be obtained from the results of this present test series:

1) The analytical expression for random beam degradation with laser propagation normal to two-dimensional turbulent mixing layers,

$$\frac{\Delta I}{I_o} = 2\left(\frac{2\pi}{\lambda}\right)^2 \alpha^2 \Delta n^2 L\ell,$$

is verified by measurements.

2) From the expression above, we see that three methods can be adopted to reduce beam degradation:

   a) reducing $L\ell$ by fluid mechanical means,
   b) reducing Δn by using other laser gases (see Ref. 3, Appendix E),
   c) Introducing multiple layers (see Ref. 3).

3) If Δn is fixed, fine-mesh screens positioned over the flow plate are quite effective in reducing $L\ell$. The growth of the mixing layer is reduced roughly by one-half with the use of a 150-mesh screen. This means beam degradation is reduced by a factor of about four. Mixing layer bending is also avoided by using the screened flow plate.

4) Higher velocity shear increases the mixing layer growth. The growth rate is a function of

$$R = \frac{U_1 - U_2}{U_1 + U_2}$$

The growth rate for a layer with $|R| \gtrsim 0.1$ is about 5% if a screened flow plate is used.

5) Exposure of a free stream to a stagnant region sufficiently far away from the mixing layer does not have an appreciable effect on the mixing layer characteristics.

Beam degradation due to turbulent mixing for the ABEL device with $\Delta n = 1.82 \times 10^{-4}$ can now be calculated. The results for a screened flow plate as in Figure 11, with $\Delta n = 1.86 \times 10^{-4}$ and

R = 0.06, can be used directly. For the same value of R, if the mixing layer height in the flow direction is 30 cm, the average beam degradation* is 0.133 x $(2\pi)^2$ for λ = 5260 Å. In the case of the ABEL CO_2 laser with λ = 10.6 μm, the beam degradation for each mixing layer is

$$\frac{\Delta I}{I} = \psi'^2 = (0.133) \times (2\pi)^2 \times \left(\frac{0.526}{10.6}\right)^2 = 1.3\%$$

The total degradation of the laser beam due to the shear layers is thus about 4.1% since the beam passes 1.6 times through the two end layers.[3] This random degradation appears sufficiently small to be acceptable.

*For shear layers, the average beam degradation between x_1 and x_2 is $\psi'^2_{av} = (\psi'^2_1 + \psi'^2_2 + \psi'_1 \psi'_2)/3$ where subscripts "1" and "2" denote values at x_1 and x_2, respectively.

REFERENCES

1. Born, M. and Wolf, E., Principles of Optics, Permagon Press, 1975, pp. 463-465.

2. Vu, B.T., Sutton, G., Theophanis, G. and Limpaecher, R., "Laser Beam Degradation Through Optically Turbulent Mixing Layers," AIAA Paper 80-1414, 13th AIAA Fluid and Plasma Dynamics Conference, Snowmass, Colorado, 1980.

3. "Cold Flow Electric Laser Development (U)", ABEL I Final Technical Report for Period 1 Jan. 1977 - 30 Sept. 1979, Army MICOM Contract DAAK40-75-C-1272, AERL Doc. 79-320, October 1979. CONFIDENTIAL

4. Brown, G.L. and Roshko, A., "On Density Effects and Large Structure in Turbulent Mixing Layers," J.F.M. Vol. 64, 1974, pp. 775-816.

5. Bendat, J.S. and Piersol, A.G., Random Data: Analysis and Measurement Procedures, J. Wiley & Sons, p. 68, 87, 288, (1971).

6. Batt, R.G., "Turbulent Mixing of Passive and Chemically Reacting Species in a Low-Speed Shear Layer," J.F.M., Vol. 82, 1977, pp. 53-95.

7. Sabin, C.M. "An Analytical and Experimental Study of the Plane, Incompressible, Turbulent Free-Shear Layer With Arbitrary Velocity Ratio and Pressure Gradient," Trans. ASME. D. 87, 1965, pp. 421.

8. Abramovich, G.N., The Theory of Turbulent Jets, M.I.T. Press 1963.

9. Kuchemann, D. and Sterne, L.H.G., (1964), Progress in Aeronautical Sciences, V5; "The Design of Low Speed Wind Tunnels," p. 12, 13, 28, 29, 30, 31.

APPENDIX A

THE OPTICAL SCIENCES CENTER CODE FOR INTERFEROGRAM ANALYSIS, "FRINGE"

The FRINGE code is an interferogram analysis program capable of handling either straight or circular fringes. Straight fringes do not have multiple values when a line is drawn nearly perpendicular to the fringe. The circular fringes have no multiple values along a radius from the pupil center or center of symmetry.

The program reads in an array of (x,y) points representing the fringe maximum or minimum and has mnemonic codes to tell the computer when fringes are missing (i.e., on edge of pupil or in central obstruction). The program has a very flexible and easily used input control format and output option selection. Internally the program takes the (x,y) array points and first fits them to a polynomial of the form

$$f(x,y) = Ax + By + C + D(x^2 + y^2) \qquad \text{(A-1)}$$

The first three terms represent the tilt while the last term give the defocus. The magnitude of D represents the defocus in waves at the edge of the pupil. The fit (x,y) is obtained via a least-squares routine and represents the fringe order. The difference between the fit and the stored array of data yields the phase errors, i.e.,

$$OPD_i = ORD_i - f(x,y) \qquad \text{(A-2)}$$

where OPD_i is the optical path difference at point i in the matrix and ORD_i is the fringe order at point i and $f(x_i, y_i)$ is the value of the polynomial fit to the data.

For straight fringes, aberration terms such as astigmatism and third-order coma can be added to the polynomial either separately or together. If this option is selected, the phase errors or residuals from the least-squares fit will be relative to this higher-order polynomial. For the circular fringe case, tilt and defocus are removed and, if desired, polynomial terms up to 10th order are fit to the data. The conic constants can be solved for or specified as desired. The program has an option to average several interferograms or subject a baseline. This is important if the effects of the measuring devices are to be removed.

There are several plotting options. Currently implemented are three-dimensional isometric plots and contour maps. Line printer contour maps are also obtainable but not used.

In summary, this program has the capability to analyze interferograms. Phase error plots are produced and polynomial coefficients representing wave aberrations are generated. Both straight and circular fringes can be handled.

APPENDIX B

RELATION BETWEEN KINETIC ENERGY AND PLENUM PRESSURE

The kinetic energy of a flowing stream in the laser cavity is

$$\rho V^2 = \rho a^2 M^2 \qquad \text{(B-1)}$$

where

ρ: gas density in the cavity

a: sonic velocity of the gas in the cavity

M: Mach number of the flowing gas in the cavity.

But from perfect gas law, we have:

$$\rho a^2 = \left(\frac{p}{RT}\right)(\gamma RT) = \gamma p \qquad \text{(B-2)}$$

where

p: cavity pressure

R: gas constant

T: cavity temperature

γ: ratio of specific heat capacities

From Eqs. (1) and (2), we get

$$\rho V^2 = \gamma p M^2 \qquad \text{(B-3)}$$

Now, the flow in the sonic orifice flow plate is given by

$$\rho VA = \dot{m} = A^* \left(\frac{\gamma}{R}\right)^{1/2} K \frac{P_o}{\sqrt{T_o}} \qquad \text{(B-4)}$$

where

V: gas velocity in the cavity

A: total flow plate area for uniform flow far from the flow plate or effective jetting area for jetting flow near the unscreened flow plate.

A*: sonic orifice area

K: defined as $\left(\frac{2}{\gamma+1}\right)^{\frac{\gamma+1}{2(\gamma-1)}}$

P_o: plenum pressure

T_o: gas temperature in the plenum.

For low Mach Number, we have

$T \cong T_o$ so that from Eq. (4) we get

$$M = \frac{V}{a} = \frac{A^*}{A} K \frac{P_o}{P} \tag{B-5}$$

From Eqs. (3) and (5) we get

$$\rho V^2 = \left(\frac{A^*}{A}\right)^2 \gamma K^2 \frac{P_o^2}{P} \tag{B-6}$$

which is our relation between kinetic energy and plenum pressure. We see that the kinetic energy, at low Mach number , is approximately independent of the gas temperature. For the unscreened ABEL flow plate the effective jetting area is 40.8% of the total flow plate area, so the kinetic energy in the jetting region is about six times higher than the kinetic energy in the uniform flow region.

The analysis above applied for choked flow across the orifice plate and the condition for choked flow is

$$\frac{P_o}{P} \geq \left(\frac{\gamma+1}{2}\right)^{\frac{\gamma}{\gamma-1}}$$

DISTRIBUTION LIST

Commander US Army Missile Command Redstone Arsenal, AL 35898 Attn: DRSMI-RHB, Dr. T.A. Roberts RHE, Mr. J.C. Walters RHC, Mr. K. Smith RHC, Mr. Myron Cole RHS, Dr. George Dezenberg	10 copies
Commander US Army Mobility Equipment R&D Command Ft. Belvoir, VA 22060 Attn: DRDME-R, Mr. Cooper EA, Dr. Larry Amstutz	2 copies
Defense Advanced Research Projects Agency 1400 Wilson Boulevard Arlington, VA 22209 Attn: Director, Laser Division	1 copy
Air Force Weapons Lab Kirtland AFB, NM 87117 Attn: AFWL/ARAY, LTC T. Meyer	6 copies
Defense Documentation Center Cameron Station Alexandria, VA 22314	12 copies
RSIC Redstone Arsenal, AL 35898	3 copies